1969

A photoelastic study of the stresses around an underground opening and its support system

Alphonse C. Van Besien

A PHOTOELASTIC STUDY OF THE STRESSES AROUND AN UNDERGROUND OPENING AND ITS SUPPORT SYSTEM

BY

ALPHONSE CAMILLE VAN BESIEN, 1937-

A

THESIS

submitted to the faculty of

UNIVERSITY OF MISSOURI - ROLLA

in partial fulfillment of the requirements for the

Degree of

MASTER OF SCIENCE IN GEOLOGICAL ENGINEERING

Rolla, Missouri

1969

Approved by

W. B. Vaughen Jones (advisor) James J. Scott

Peter G. Hansen

ABSTRACT

The stress conditions around openings in rock have long been of interest to the field of rock mechanics. The purpose of this investigation was to determine the stress distribution around an opening with a rib and wall-plate support system.

A photoelastic model of the opening (a modified horse-shoe section) was loaded in the centrifuge to determine the effect of body loading. Both the tangential stress and the stress within the rock bench, due to the opening, were determined. The stress conditions within the bench were examined using simulated ribs and a loading frame. Application of the data is discussed, as well as the relative importance of the various stress concentrations. It is concluded that a zone of tensile stress within the rock bench is the limiting factor in the design of this opening.

ACKNOWLEDGEMENT

The author wishes to express his appreciation to his advisor, Dr. Nolan B. Aughenbaugh and to Dr. James J. Scott, for their continuous counsel and support. Special appreciation is due Dr. Peter G. Hansen for his assistance with photoelasticity and to Dr. C. J. Haas.

The author wishes to express his gratitude to Col. Edwin R. Decker, and others of the St. Louis District of the Corps of Engineers, whose cooperation made this graduate study possible. Finally, the author is indebted to his wife, Carol, for encouragement and patience during the past year.

TABLE OF CONTENTS

LIST OF PHOTOGRAPHS

LIST OF FIGURES

LIST OF TABLES

I. INTRODUCTION

One of the principal areas of interest within the field of rock mechanics lies in the study of the stress changes produced by the introduction of a tunnel or opening into a rock mass. Stress distributions around openings of various shapes in a uniformly stressed, semi-infinite, elastic medium, have been studied using theory of elasticity and, for more complex shapes, photoelasticity. In most studies, however, the effect of a tunnel support system on the stress distribution has been neglected. This paper represents an attempt to study the combined effects of an opening and its support system on a portion of the rock mass.

A relatively common support system, used when light roof loads are anticipated, is the rib and wall plate type (Proctor and White, 1946). This system (Fig. 1) consists of a semicircular steel rib, used to support the crown of the tunnel, resting on a horizontal steel beam or wall plate which, in turn, rests on a "hitch" or bench cut into the side of the tunnel at some elevation above the invert. The rib and wall plate system was developed to reduce costs by eliminating both the need for steel posts extending to the tunnel invert and the extra rock excavation to provide the space necessary for the steel posts. However, it can be successfully used only when the rock is relatively sound and the roof loads are light.

In spite of its apparent economic advantages, the rib and wall plate system of support is gradually falling into disuse, chiefly due to problems encountered during construction. All too frequently during construction, it is found the rock bench or hitch is not capable of supporting the steel ribs or the roof load and costly changes must be made in the tunnel support system. In some instances failure of the rock bench is due to blasting

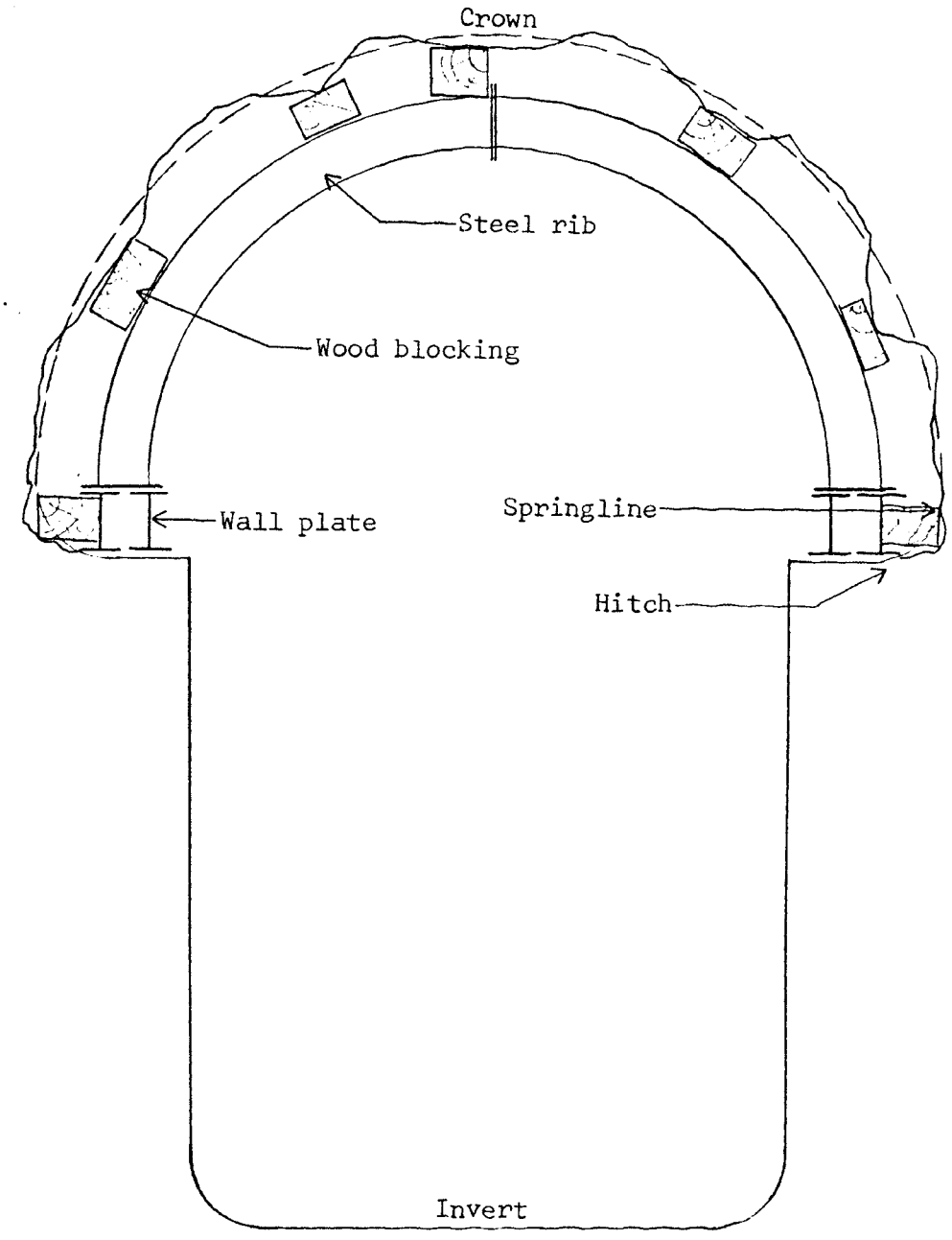

Figure 1. Rib and wall plate support system.

damage. In other cases, failure has been attributed to stress relief or stress concentrations created in the rock mass by the tunnel configuration or by the support system. A photoelastic model study of the stress conditions around such an opening may provide data with which to evaluate the suitability of the design for a particular site or rock condition.

II. PREVIOUS WORK

A. Theoretical Solutions

Obert and Duvall (1967) presented brief summaries of two methods, Greenspan (1944) and the complex variable method, for obtaining the theoretical solution to the stress distribution around a single hole in a plate. The Greenspan method will obtain an exact solution for any opening whose boundary can be expressed as

$$x = p \cos B + r \cos 3B$$

$$y = q \sin B - r \sin 3B$$

where p, q, and r are parameters and B is an angle. From the general equation for the tangential stresses at the boundary of a hole (page 115, Obert and Duvall, 1967) the following expression can be derived for a plate with a vertical stress field:

$$\frac{S_t}{S_y} = \frac{F \sin^2 B + G}{A \sin^2 B + K \cos 2B + C}$$

where $S_y \neq 0$

$S_x = T_{xy} = 0$

S_t = tantential stress

$A = (p - q)(p + q - 6r)$

$C = q^2 + 6rp + 9r^2$

$$F = (p + q)\left[(p - q) - \frac{2p\,(p + q - 6r)}{p + q - 2r}\right]$$

$$G = (q - 3r)\left[(q + 3r) + \frac{2p(p + q)}{p + q - 2r}\right]$$

$K = -6r\,(p + q)$

and B, p, q, and r are as previously defined.

Heller, Brock, and Bart (1958) employed the complex variable method

to determine the stress distribution around rectangular openings with rounded corners. The complete solution is, of course, too lengthy for presentation in this study. An important feature of this report was the determination of stress concentrations at the corners of rectangular openings. For a unidirectional stress field (S_y) and a square opening:

$$\frac{S_t}{S_y} = 3.8$$

where $\frac{r}{H_o} = \frac{1}{16}$

r = radius of corner fillet

H_o = height of opening

From these and other theoretical solutions, Obert, Duvall, and Merrill (1960) arrived at the following general conclusions:

> 2. With a unidirectional vertical stress field, a stress concentration of approximately -1 is developed in the roof, that is, the stress in the roof is tension and is equal to the applied compressive stress.
>
> 7. In any type of stress field sharp corners on an opening will produce high stress concentrations and should be avoided.
>
> (OBERT, DUVALL, and MERRILL, 1960, p. 17)

B. Photoelastic Solutions

Panek (1951) conducted a photoelastic study of the stress distribution around rectangular openings with rounded corners, varying both the width-to-height ratio and the attitude of the opening in relation to the stress field. Results indicated that the magnitude of the critical stress concentrations increased as the W/H ratio increased, with the maximum stress concentrations occurring when the openings were oriented at 45° from a uniaxial stress field. Critical tensile stress concentrations

decreased as the ratio of the horizontal stress to the vertical stress increased. When the horizontal stress was equal to the vertical stress, no tensile stresses were generated.

Phillips and Zanger (1952) presented the theoretical stress distribution for a circular hole in a plate and compared this with the stresses computed from a photoelastic study of the same model. Having demonstrated the validity of the photoelastic technique, Phillips and Zanger then presented the results of a photoelastic study of a gallery similar to those formed within concrete dams. The opening studied was horse-shoe shaped with straight vertical sides and sharp corners at the junction of sides and floor. For a uniaxial vertical stress field, the maximum tensile stress was generated at the crown of the opening and was equal to approximately $-1.1\ S_v$. Extremely high stress concentrations were induced at the corners of the opening. The maximum tensile stress generated on the base of the opening (excluding corners) was $-1.0\ S_v$ and was uniform across most of the floor of the opening.

A study of a similar opening was presented by Abel (1967). A maximum tensile stress of $-0.9\ S_v$ was reported at the crown of the tunnel; the tensile stresses at the center of the tunnel invert were approximately $-0.6\ S_v$. The maximum compressive stress was observed at the tunnel springline and was of the order of $+2.3\ S_v$.

Nair and Udd (1965) presented photoelastic solutions for multiple ovaloidal openings in plates for uniaxial stress conditions. The technique of superposition was employed to determine the effect of biaxial stress conditions. Of particular interest (and some controversy) was the observation that the greatest tensile minor principal stress occurred at a point removed from the boundary of the openings.

C. Tunnel Support Systems

The most exhaustive treatment of tunnel support systems is that by Proctor and White (1946). Although basically empirical in nature, the criteria presented are those most widely used in the construction industry and have served as the basis for many later studies of tunneling systems. Of particular interest is the treatment of rock classification as related to roof loads, developed by the late Dr. Karl Terzaghi. This analysis of the loads imposed on tunnel supports furnished the basic concept for the loading simulated in the following study. An elastic analysis of tunnel supports based on Proctor and White was presented by Abel (1967).

III. EXPERIMENT CONCEPT

A. Basic Concepts

1. Design of the Opening

The selection of the rib and wall plate support system was occasioned by the author's personal experience in the construction of tunnels related to the St. Louis Flood Protection Project of the U.S. Army Corps of Engineers. The opening was proportioned to be relatively high-sided, in line with the general usage of this support system. The opening selected is also of the same general proportions as that studied by Phillips and Zanger (1952), providing a convenient basis for comparison of results. The decision to use rounded corners, or fillets, was based on the author's opinion that it is virtually impossible to form sharp interior corners in rock with ordinary excavation techniques. Sharp corners which might be formed will generally deteriorate to rounded corners, because of the high stress concentrations present, under even moderate loading conditions.

2. Loading Conditions

Rib and wall plate tunnel support systems are generally used where light roof loads are anticipated. A vertical load with no lateral constraint is easily simulated and probably corresponds most closely to the stress conditions at shallow depths (Obert and Duvall, 1967, p. 495). The decision to apply the vertical load with a centrifuge rather than a loading frame was based on the desire to include, in the study, the effect of the weight of the material immediately

around the opening. Under loading frame conditions the effects of body loads are insignificant and cannot be detected, with ordinary photoelastic techniques.

B. Model Similitude Relations for the Tunnel Opening

1. Variables and π-Terms

The stress (S_p) around a prototype tunnel opening in a homogeneous rock mass, subjected only to vertical body loads, depends on the dimensions (L_p) of the opening, the elastic properties of the rock (Young's modulus = E_p; Poisson's ratio = v_p) and the unit weight of the rock (G_p). The dimensional matrix is:

	S_p	L_p	E_p	v_p	G_p
F	1	0	1	0	1
L	-2	1	-2	0	-3

where F = force

L = length

The rank of the matrix is two; therefore, the number of dimensionless products, or π-terms, is three (since there are five variables). The dimensionless products selected are:

$$\pi_{1p} = \frac{S_p}{E_p}$$

$$\pi_{2p} = v_p$$

$$\pi_{3p} = \frac{G_p L_p}{E_p}$$

2. Similitude Relations

A functional relationship can be written such that

$$\pi 1_p = f(\pi 2_p, \pi 3_p)$$

and

$$\frac{S_p}{E_p} = f\left(v_p, \frac{G_p L_p}{E_p}\right)$$

where f is an undetermined function. By replacing the subscript p with m, an equivalent relationship can be written for the model:

$$\frac{S_m}{E_m} = F\left(v_m, \frac{G_m L_m}{E_m}\right)$$

Since the model is to be loaded in the centrifuge, the functional relationship for the model can be rewritten as:

$$\frac{S_m}{E_m} = f\left(v_m, \frac{KG_m L_m}{E_m}\right)$$

where the ratio of the centrifugal load to gravity load is

$$K = \frac{4\pi^2 rw^2}{g}$$

and r is the radius and w the rotational speed (in rps) of the centrifuge.

For model-prototype similitude to exist, the following relationships must be satisfied:

$$\frac{S_m}{E_m} = \frac{S_p}{E_p}, \quad v_m = v_p, \quad \frac{KG_m L_m}{E_m} = \frac{G_p L_p}{E_p}$$

From these relationships the model scale may be developed:

$$\frac{L_m}{L_p} = \left(\frac{G_p}{KG_m}\right)\left(\frac{E_m}{E_p}\right)$$

The stress scale may be expressed as:

$$\frac{S_m}{S_p} = \frac{E_m}{E_p}$$

3. Model Material

Columbia Resin 39 (CR-39) was selected as the model material, since it possesses a relatively low fringe constant (F) and is readily available. CR-39 is easily machined and may be obtained in a variety of forms. The pertinent mechanical properties of CR-39 are:

Unit Weight (G_m) = 80.8 pcf (Experimentally determined)

Young's modulus (E_m) = 350,000 psi

Poisson's ratio (v_m) = 0.36

Yield stress = 5,000 psi (Hansen, 1969).

The stress-optic properties of CR-39 are variable and must be determined experimentally for each sample. Calibration of the model material is discussed under "Experimental Procedure".

4. Model-Prototype Similitude

Using the design equations derived previously and the physical properties of CR-39, the relationships between model properties and the properties of a hypothetical prototype can be developed. Assume an opening is to be constructed in rock with a unit weight (G_p) of 162 pcf and a Young's modulus of 7.0×10^6 psi. Poisson's ratio of the rock will be assumed equal to that of CR-39, 0.36. Poisson's ratio for rock is of this order but is extremely difficult to measure experimentally. The error introduced by non-equal Poisson's ratios is felt to be insignificant. The assumed physical properties are similar to those of many massive dolomites and limestones, including

the Eminence and Gasconade Formations of Missouri.

The following relationships exist between the physical properties of the model and the prototype:

$$G_p = 1.98\ G_m \simeq 2.0\ G_m$$

$$v_p = v_m$$

$$E_p = 20\ E_m.$$

The scale equations, previously derived, may now be written as follows:

$$\frac{S_m}{S_p} = \frac{E_m}{E_p} = \frac{1}{20}$$

$$\frac{L_m}{L_p} = \frac{2.0}{K}\ \frac{1}{20} = \frac{1}{10K}$$

$$\text{or } \frac{L_p}{L_m} = 10K$$

Assuming a rotational speed of 360 rpm (6 rps) and a radius of 2.58 feet (Fig. 2), the ratio of centrifugal to gravity loading is:

$$K = \frac{4\pi^2 rn^2}{g} = 114$$

Under these conditions

$$L_p = 1{,}140\ L_m$$

$$S_p = 20\ S_m.$$

5. Use of Steel Weight

Ideally, the vertical stress on the model could be generated solely by the weight of the overlying plastic. In practice, this is not possible; the size of the centrifuge rotor arm limits the dimensions of the model. Also, the effective weight of the overlying model

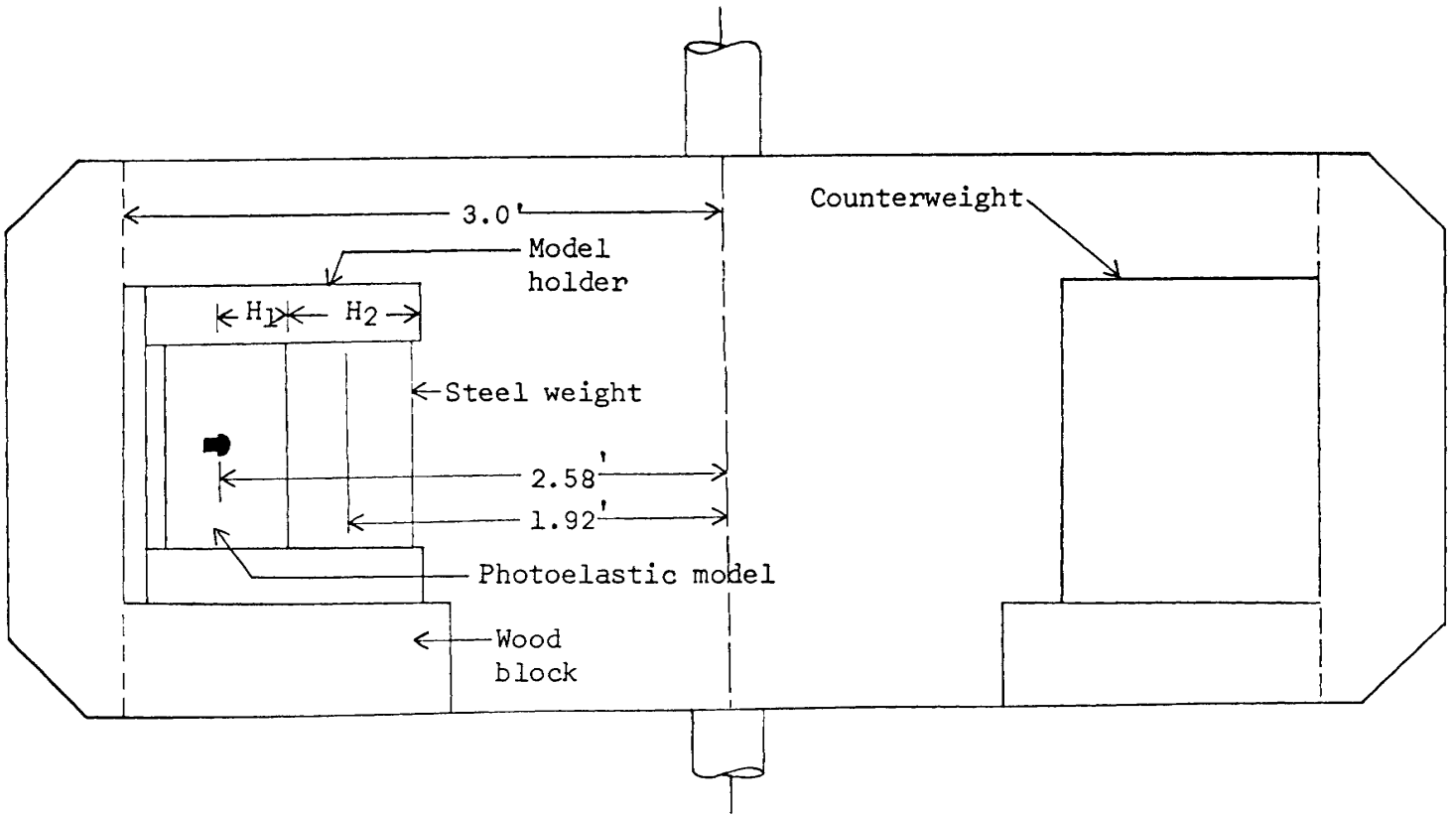

Figure 2. Centrifuge rotor arm and model.

material decreases to zero as the material approaches the center of the centrifuge.

The stress created by overlying rock was simulated by the addition of a steel weight to the top of the model. Having a much higher density than the plastic, the steel could simulate a much greater depth of burial than a comparable height of CR-39.

Without the steel weight, the vertical stress at the same elevation as the top of the bench in the opening would be equal to the effective unit weight of the overlying plastic multiplied by the height of the overlying material:

$$S_v = K_1 G_m H_1$$

$$\text{where } K_1 = \frac{4\pi^2 r_1 w^2}{g} . \qquad \text{(Figure 2)}$$

With the addition of the steel weight

$$S_v = K_1 G_m H_1 + K_2 G_s H_2$$

$$\text{where } K_2 = \frac{4\pi^2 r_2 w^2}{g} .$$

Since the ratio of the effective weight of the CR-39 to the effective weight of the steel is:

$$\frac{K_1 G_m}{K_2 G_s} = \frac{r_1 G_m}{r_2 G_s} = \frac{1}{4.48}$$

the addition of eight inches of steel weight is equivalent to the addition of 35.8 inches of plastic, at the same radius of rotation.

6. Dimensions of the Opening

The model opening was 1.70 inches in height. Since $L_p = 1{,}140\ L_m$, the prototype opening would be 1,940 inches, or 162 feet, in height.

This corresponds with the dimensions of excavations for underground powerhouses. The ratio $\frac{S_p}{S_m}$ is of significance only to the extent that it shows a direct proportionality between the stresses in the model and the prototype. For the remainder of this study, the stresses in the model will be compared to the vertical stress without the model opening. Since the ratio between S_p and S_m is constant, the comparison between the stresses around the opening and the vertical stress will be valid for the prototype.

C. Simulation of Rib Loading

1. Basic Assumptions

As indicated in Proctor and White (1946), the magnitude and direction of the rib load is controlled by the roof load and the location of blocking. Assuming a symmetrical roof load and that the steel ribs are vertical where they meet the rock bench, the rib load may be separated into two components. The large vertical component is controlled primarily by the roof load. The smaller horizontal component is controlled by the location of the nearest blocking point. Since it was not feasible to install model ribs and blocking in the opening, the loading was simulated by applying a force inclined at 6° from the vertical to simulate average blocking. The inclined load was applied over the entire horizontal surface of the bench, rather than as a point load.

2. Similitude

Rib loading was to be accomplished in the loading frame rather

than in the centrifuge. Since no additional scaling was required because of centrifugal loading, the similitude of the model and prototype is governed only by the relative dimensions of the two openings. Thus, the stress distribution in the model can be applied to any opening of the same proportions, including the opening simulated in the centrifuge. The effect of body loads has already been included in the simulation of the stresses around the opening so it is not necessary to include body weight in the simulation of the rib loading.

IV. EXPERIMENTAL PROCEDURE

A. Calibration of Model Material

The fringe constant (F) of CR-39 varies from 85 to 120 psi/fringe/inch and, consequently, each sample must be individually calibrated if quantitative results are to be obtained. Using excess material removed from the top of the model, a beam was fashioned and loaded as shown in Figure 3. The load was gradually increased and as successively higher fringes appeared at the edges of the beam, the loads were recorded.

At the center of the beam, the portion in pure bending:

$$S_2 = 0$$

$$S_1 = \pm \frac{\frac{P}{2} a \frac{h}{2}}{\frac{bh^3}{12}} = \pm \frac{3Pa}{bh^2}$$

The fringe constant is defined as

$$F = (S_1 - S_2) \frac{b}{n} ,$$

where b is the thickness of the beam and n is the fringe order. Therefore:

$$F = \left(\frac{3Pa}{bh^2}\right)\left(\frac{b}{n}\right)$$

$$F = \frac{3Pa}{h^2 n} .$$

Usually, however, it is more accurate to graph P vs. n (Figure 4) and determine the slope of the line:

$$P = \left(\frac{3a}{h^2}\right)\left(\frac{\Delta P}{\Delta n}\right).$$

Using the above technique, the fringe constant of the material being used for this study was determined to be 108 psi/fringe/inch.

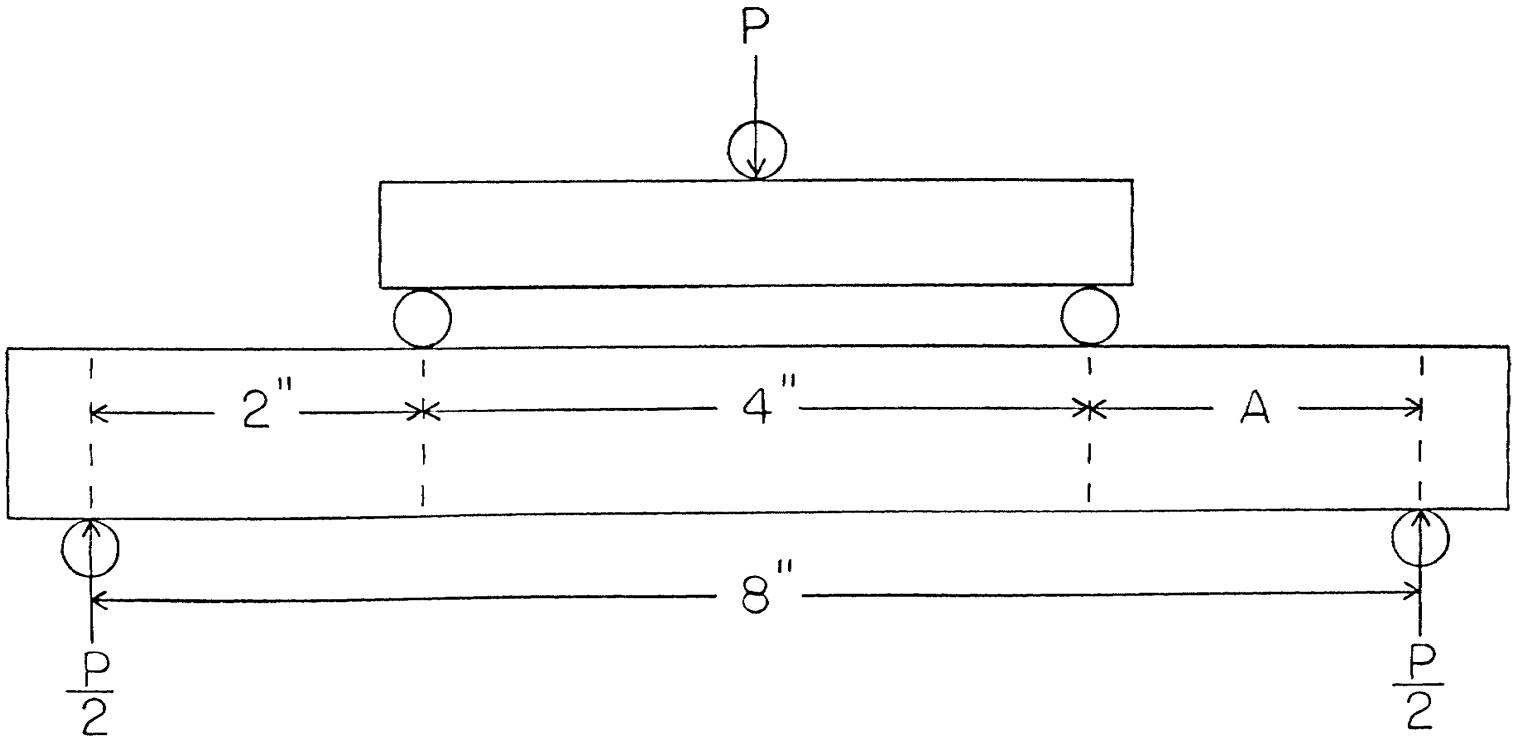

Figure 3. Calibration test device.

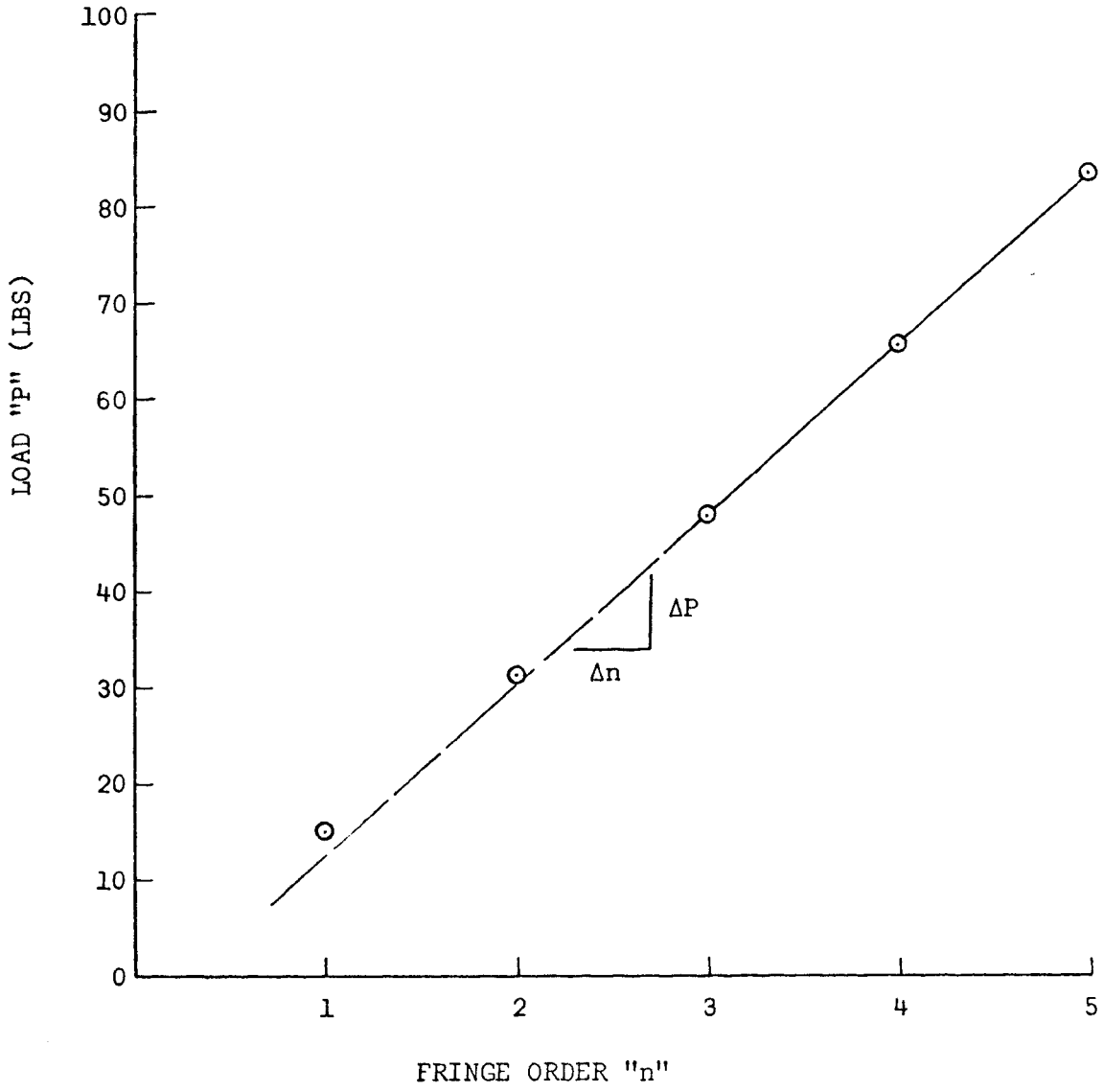

Figure 4. Calibration test curve.

B. Model Production

The first step in the manufacture of the model opening was to produce a template of the required shape from 1/8 inch aluminum sheet stock. The completed template was placed in the desired position and secured to a sheet of CR-39 with double faced cellophane tape. Since the opening was to be cut with a side-milling router, it was necessary to drill a 1/2 inch drill hole through the center of the opening to gain access for the router bit. The opening was to be considerably larger than the drill hole so only minimum precautions were necessary to prevent heating or chipping. Initially, the corner fillets were formed by hand filing after routing out the rest of the opening. Later it was found that better results were obtained by drilling small holes of the desired radius at the corners of the opening and then routing out the opening. In drilling through the plastic, the best results were achieved by using a very rapid rotation and penetration rate, with numerous pauses to prevent heating of the plastic. The plastic tended to chip when the drill bit emerged; this can be minimized by placing the model on a smooth wood surface, such as a bread board. The principal difficulties encountered in routing were the tendency of the router to cause chipping when cutting around inside corners and the tendency of the router to create heat stresses in the plastic. The latter can be minimized by using a new, sharp, router bit.

C. Testing Technique

1. Model Holder

The completed model and steel weight were larger than any models previously tested in the UMR centrifuge. A new and larger model holder

was designed and built for this study. The holder was slightly larger than the centrifuge access port (Figure 5) so final assembly was accomplished inside the centrifuge. The assembled model holder (Figure 6) was secured in the rotor arm by means of wood blocks and wedges. The centrifuge was balanced by installing a counter weight in the other arm of the rotor. The counterweight was manufactured from a previously used model holder with the addition of steel weights.

2. Centrifuge Testing

After the completed model had been examined for heat fringes due to milling (see Photograph 1), it was placed in the centrifuge and the centrifuge was sealed and evacuated. When the centrifuge had reached a speed of 300 rpm (the model cannot be viewed at lower speeds due to failure of the synchronous light to "stop" the model) the model was examined to see if it was being properly loaded. The top and bottom edges of the model being out of parallel by as much as 0.02 inches in 12 inches resulted in an obviously asymmetrical fringe pattern.

Some difficulty was encountered in eliminating what appeared to be point loads along the top and bottom edges of the model. Repeated grinding of the edges and cleaning of the model holder failed to remove some of the stress concentrations. Some improvement was obtained by placing thin (1/20") sheets of cardboard between the model and the holder and between the model and the steel weight. The edge stresses which remained are believed to be caused by fractional-order (< 0.5) heat stresses created during routing, rather than by point loading.

After several attempts, a satisfactory load distribution was

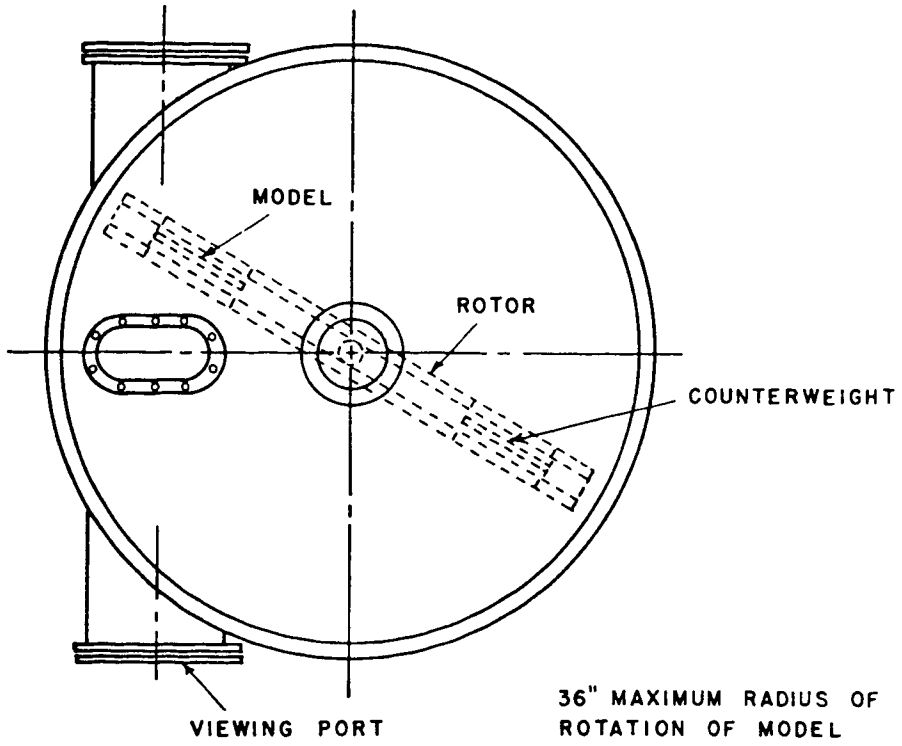

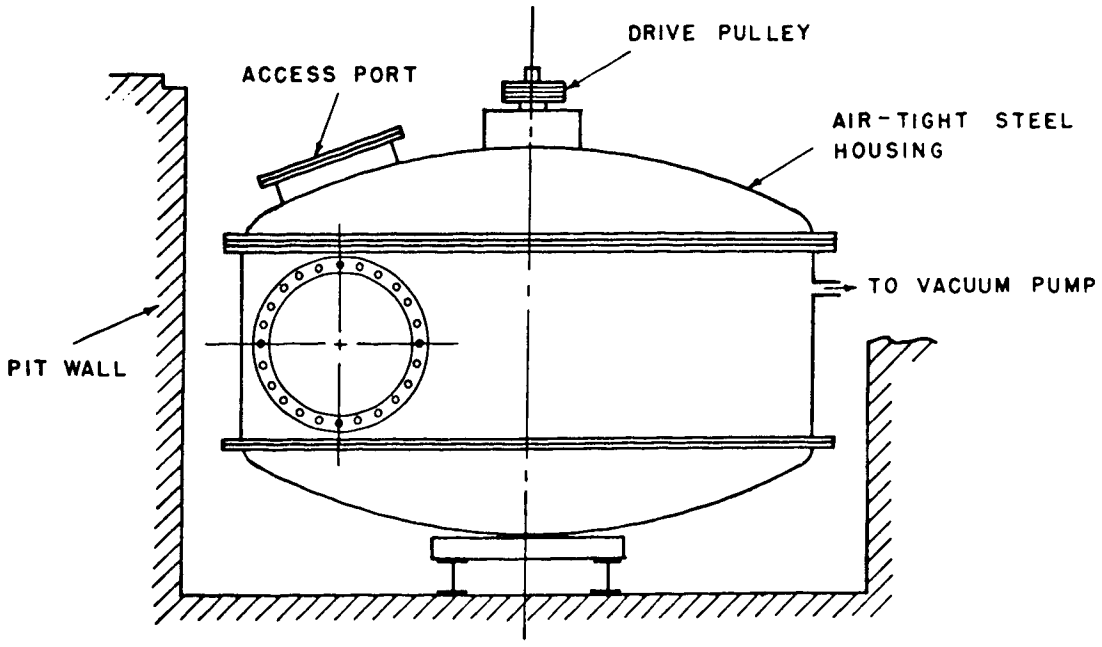

Figure 5. Centrifuge (after Haas, 1963).

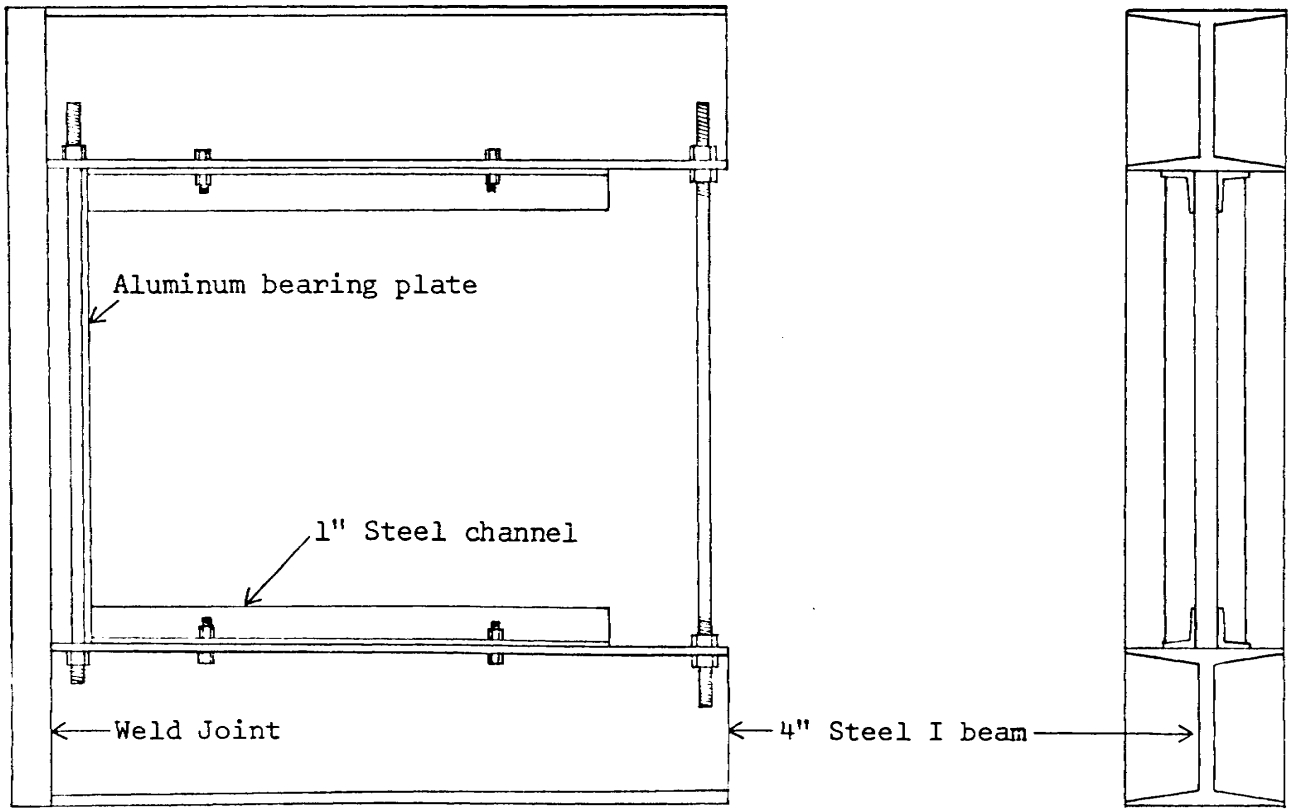

Figure 6. Model holder.

obtained and the centrifuge speed was increased to 360 rpm. The isochromatics* were observed and photographed (Photographs 2-6, Appendix A). Due to the relatively weak lighting of the model, it proved to be impossible to obtain satisfactory photographs of the isoclinics*, using the centrifuge. After several fruitless attempts (Photographs 7 and 8), the isoclinics were finally obtained by loading the model in the loading frame (Photographs 9-14).

3. Loading Frame Testing

As previously indicated, the loading frame was used to calibrate the model material and to obtain the isoclinics caused by vertical loading of the model. The loading frame was also used to simulate the rib loading (Photographs 15-22). The only difficulty encountered was in obtaining sufficient load to cause distinct fringe patterns.

D. Photography

Polaroid Polapan type 52 film was used for all photography. The only disadvantage of this film is the lack of negatives for reproduction purposes. The camera used in centrifuge testing was that supplied with the Chapman Photoelastic Polariscope. A Graphex camera was used during loading frame testing. Table I in Appendix B provides pertinent photoelastic and photographic data for all photographs.

---

*See Appendix C for definitions of photoelastic terms.

V. RESULTS OF EXPERIMENT

A. Stress Distribution Around Opening

Figures 7 and 8 were prepared from Photographs 2-14 and show the isoclinics and isochromatics for the stress distribution around an opening in a vertical stress field. Stress trajectories are shown in Figure 9.

Since the maximum stress concentrations created by any opening occur at the boundary of the opening (Obert and Duvall, 1967), an examination of the tangential stress at the edges of an opening will reveal the critical stress concentrations that affect the stability of an opening (in homogeneous elastic rock). At the boundary of an opening the radial stress is always zero so that

$$S_1 - S_2 = S_t - S_r = S_t.$$

Thus, at the boundary of an opening, the tangential stress can be computed directly from the fringe order (n) and the stress-optic properties of the model:

$$S_t = \pm \frac{Fn}{b}$$

It is convenient to compare the values of the tangential stress with the vertical stress which would have existed in the model without the opening. The vertical stress at the same elevation as the top of the bench was previously determined as:

$$S_v = K_1 G_m H_1 + K_2 G_s H_2$$

$$\text{or } S_v = 214 \text{ psi when } w = 6 \text{ rps}.$$

Since $\frac{F}{b}$ is a constant for the model and is 216 psi, the ratio of $\frac{S_t}{S_v}$ is the same as the fringe order:

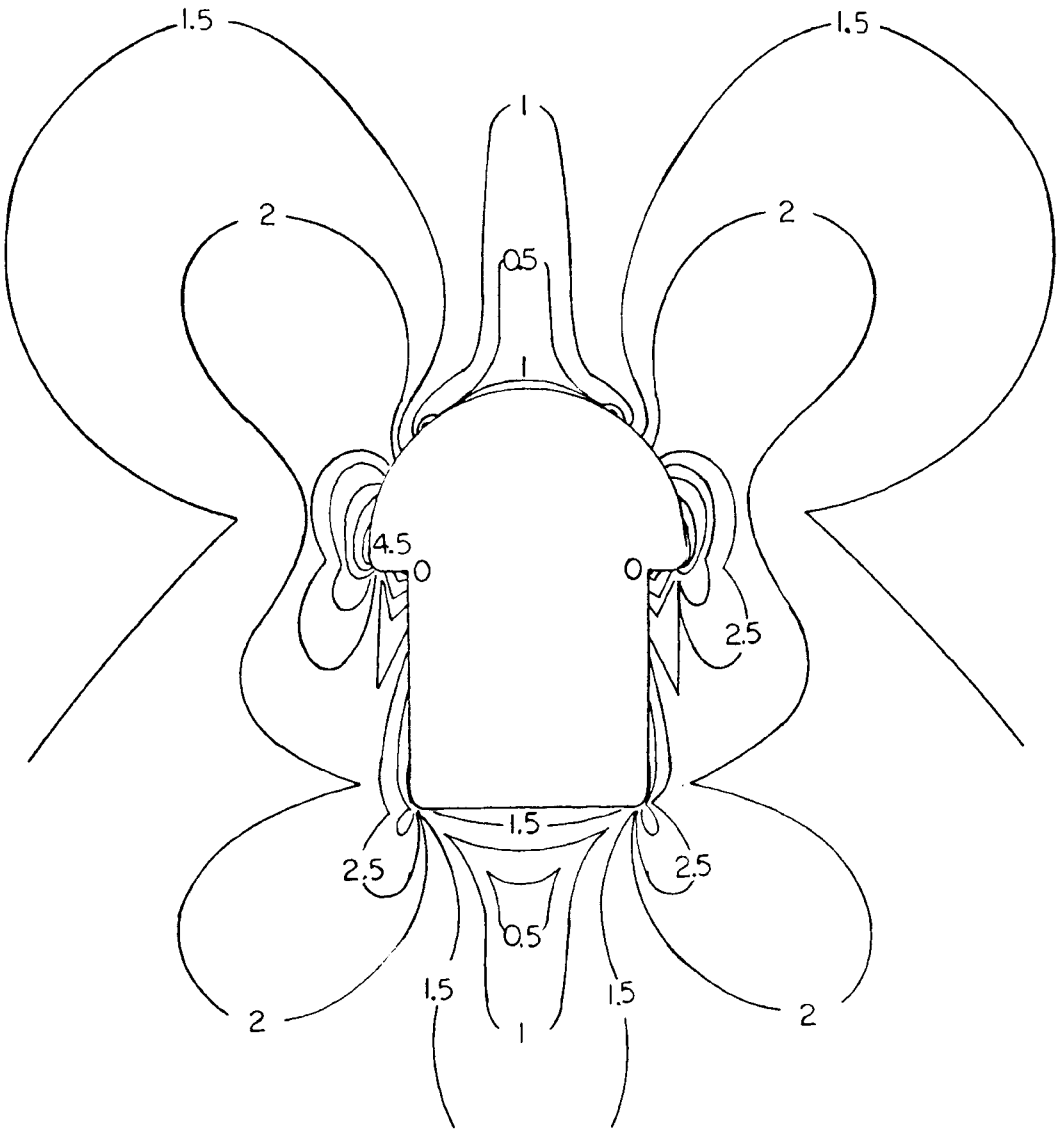

Figure 7. Isochromatics for stress distribution around tunnel opening.

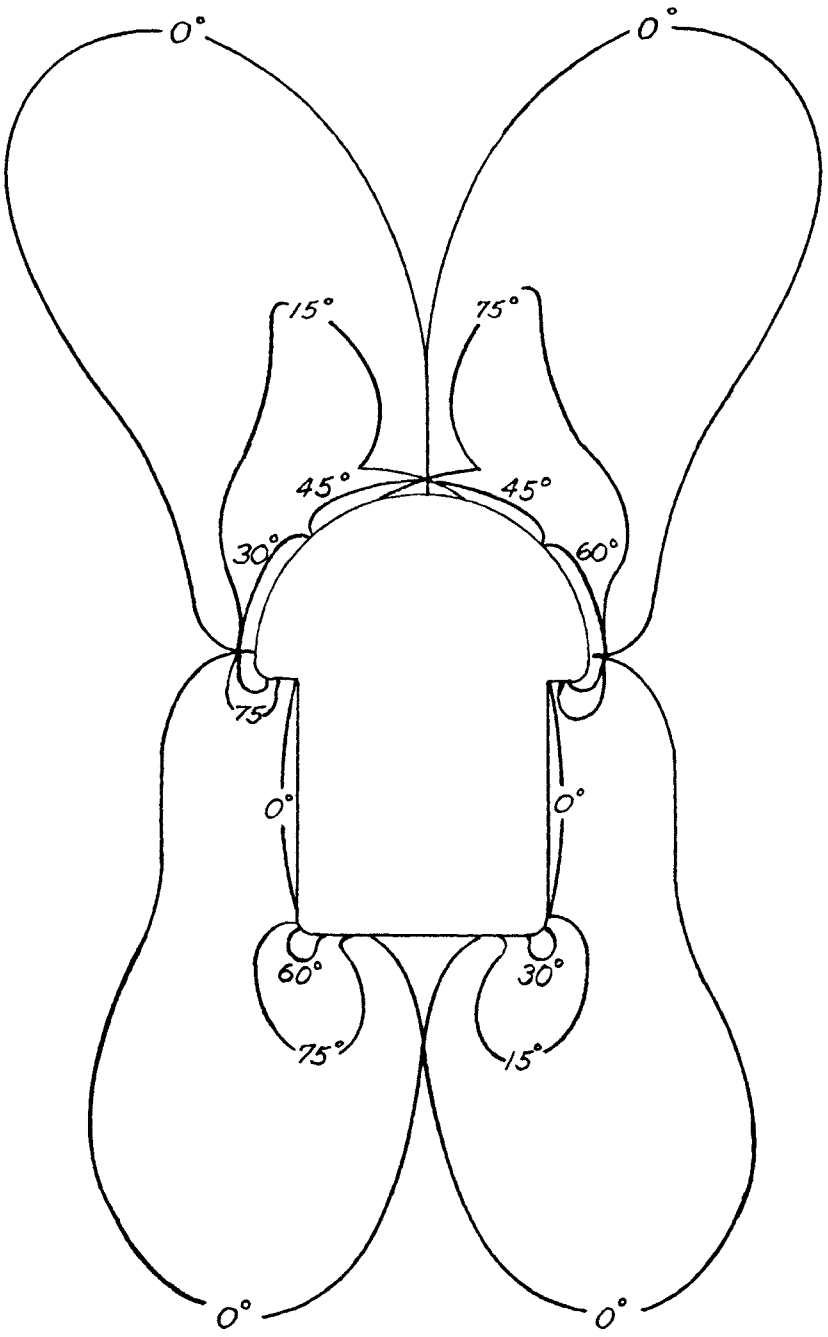

Figure 8. Isoclinics for stress distribution around tunnel opening.

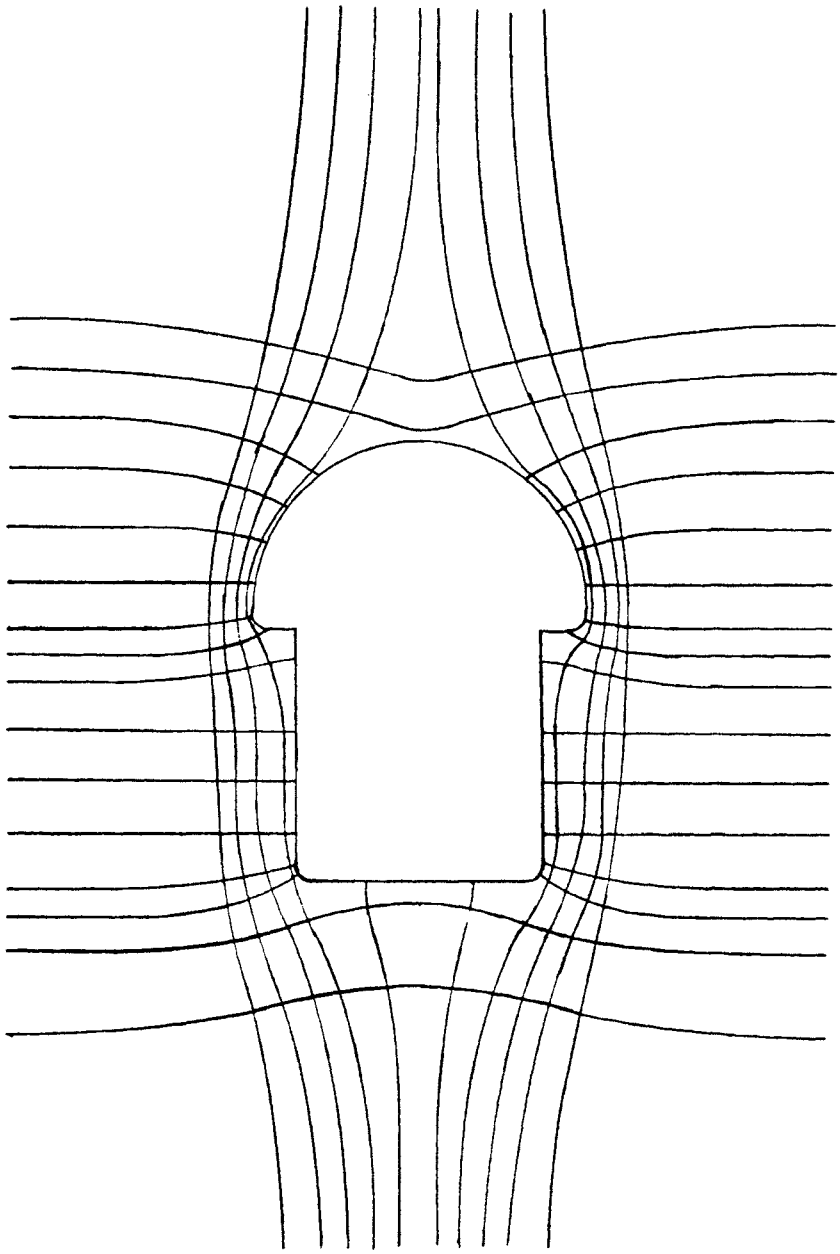

Figure 9. Stress trajectories for stress distribution around tunnel opening.

$$\frac{S_t}{S_v} = \frac{\frac{F}{b}n}{214} = \frac{216n}{214} \simeq n$$

The ratio of the tangential stress to the bench-top vertical stress is shown in Figure 10. (Note that the outline of the opening is the dividing line between tensile and compressive stresses.) As indicated, tensile stresses equal to approximately -1 S_v are generated at the crown of the opening and stresses of -1.5 S_v occur on the floor of the opening. The maximum tangential compressive stress occurs at the springline of the opening and is approximately +4.5 S_v. The maximum compressive stress at the lower fillets is +3.5 S_v. Points where the sign of the tangential stress changes are indicated by the location of zero-order isochromatics, by the location of isotropic points on the boundary of the opening or by changes in the relation of the stress trajectories to the boundary of the opening, either intersecting or parallel to the boundary.

The tensile stress in the crown of the opening (-1 S_v) compares well with that determined by Phillips and Zanger (1952) for a horse-shoe shaped opening. The higher tensile stress reported on the floor of the opening is probably the result of increased vertical stress due to the weight of the overlying material, i.e. the result of body loading. Heller, Brock and Bart (1958) reported stress concentrations of 3.35 and 3.8 for fillets whose ratios of radius to the width of the opening were 1/8 and 1/16 respectively. Interpolating for an opening where r/w = 1/12, the value of +3.5 S_v obtained in this report appears to be reasonable. The maximum compressive stress of +4.5 S_v at the springline corners does not compare with the value of +2.75 reported by Phillips and Zanger (1952). It is interesting to note that Obert and Duvall (1967) report a stress of 5.0 S_v at the narrow end of an ellipse with a width to height ratio of two

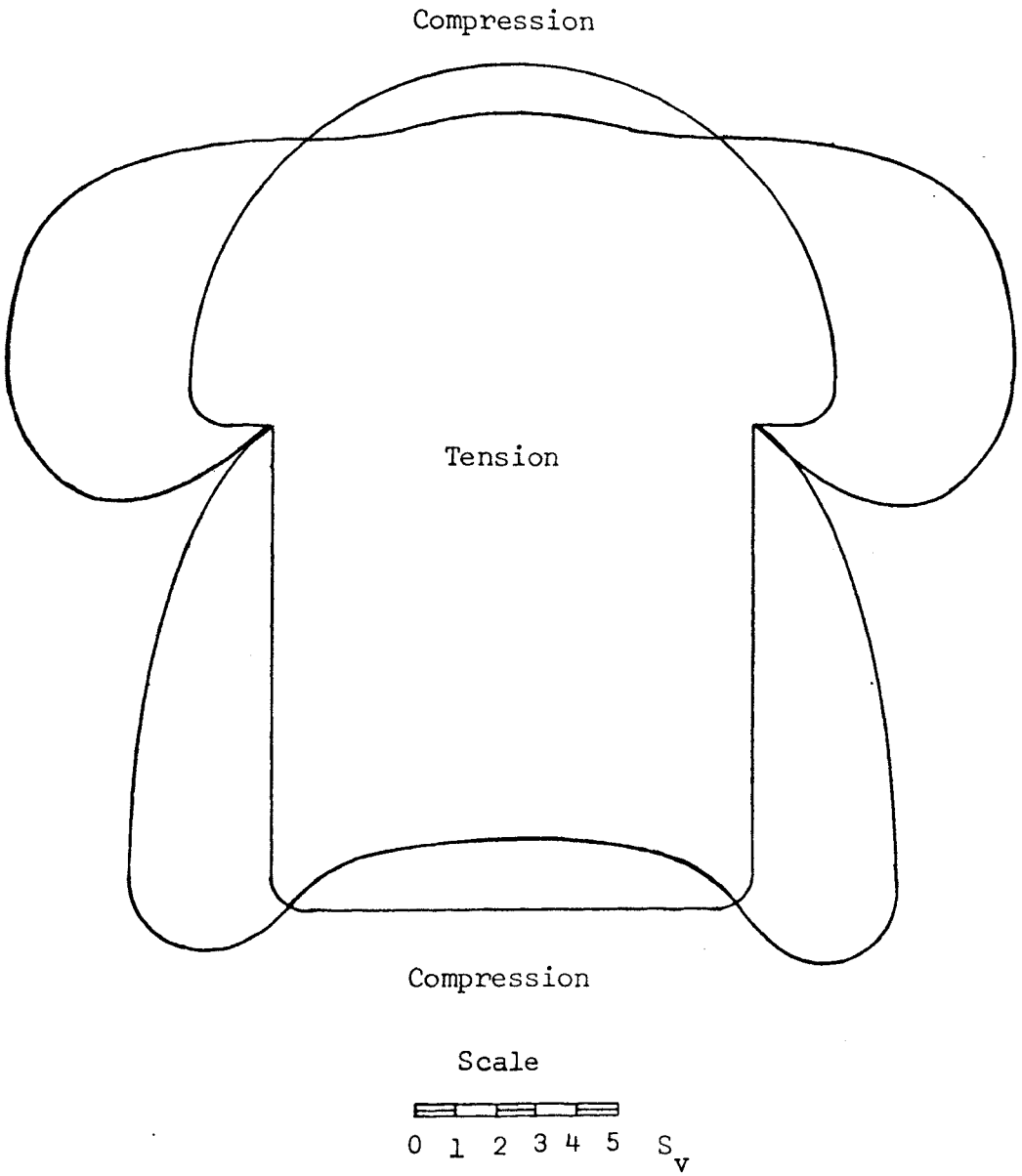

Figure 10. Tangential stress at the boundary of the opening.

oriented with the long axis at right angles to a vertical stress field.

B. Stress Distribution in Bench

1. Shear Difference Method

The evaluation of the stresses within the bench, required the use of the shear difference method (Chapter 8, Frocht, 1941). The shear stress, T_{xy}, at any point on an arbitrary straight line, can be evaluated from the photoelastic data by the equation:

$$T_{xy} = \frac{(S_1 - S_2)}{2} \sin 2\theta = \frac{(S_1 - S_2)}{2} \sin 2\theta'$$

where the angles θ and θ' are furnished by the isoclinics. The angle θ' is defined as the acute angle measured from the normal of the plane of T_{xy} to the algebraically maximum principal stress. If points 0 and P lie on the same straight line then

$$(S_x)_p = (S_x)_o - \int_0^P \frac{\delta T_{xy}}{\delta y} \delta x$$

$$\text{and } (S_x)_p = (S_x)_o - \Delta T_{xy} \frac{\Delta x}{\Delta y}$$

For convenience, Δx was made equal to Δy, so that the last equation becomes:

$$(S_x)_p = (S_x)_o - \Delta T_{xy}$$

2. Results of Analysis

The stress distribution, in terms of the vertical stress, is shown in tabular form in Table II and in Figure 11. Of prime importance is the fact that relatively high compressive stresses

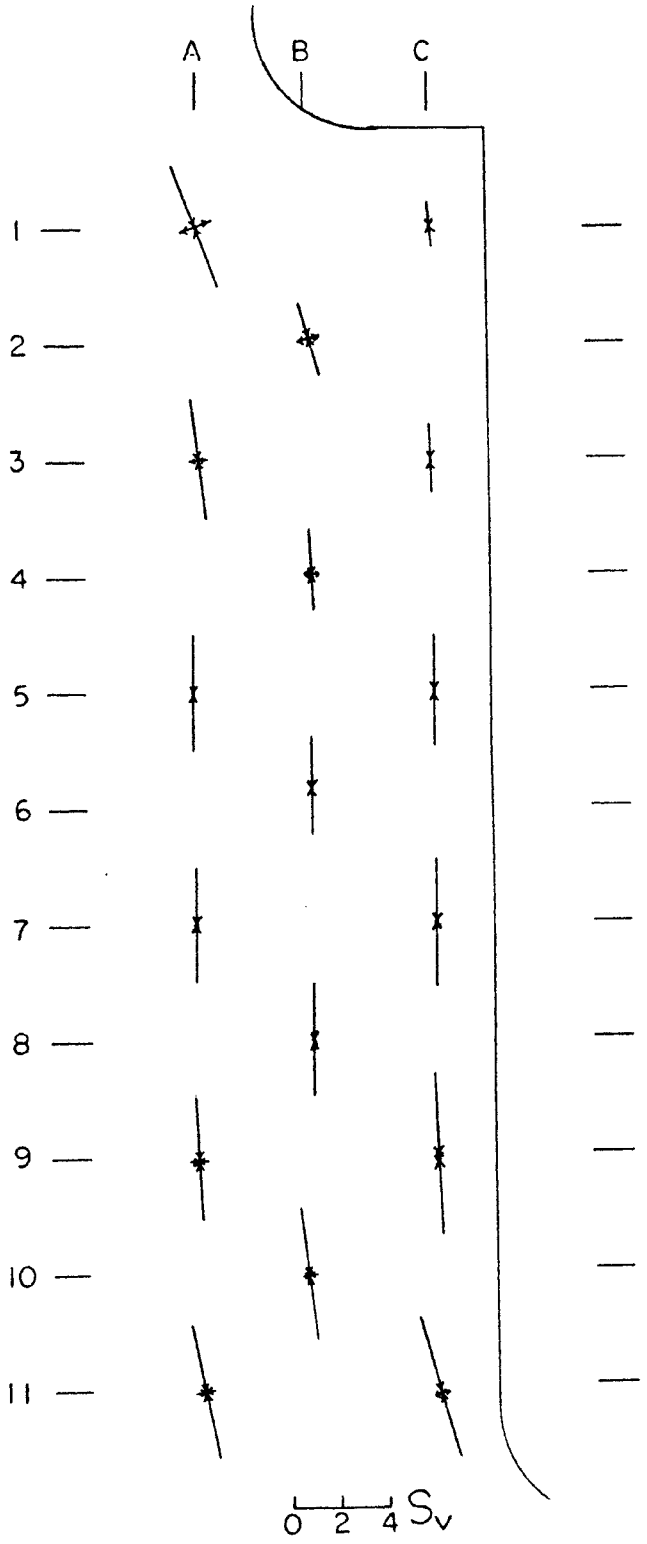

Figure 11. Bench stresses due to opening.

occur near the top of the bench. The occurrence of a zone of tensile minor principal stresses in the upper one-third of the bench is also significant. The angle θ refers to the angle between one of the principal stresses and the vertical or horizontal axes, and is measured in a clockwise direction.

C. Stress Due To Rib Loading

A contact pressure of 1000 psi was exerted by each simulated rib, at an angle of 6° from the vertical. As indicated by the isoclinics and the stress trajectories (Figures 12 and 13) the orientation of the stresses within the bench was largely controlled by the proximity of a vertical free surface. Some concentration of stresses may be observed along the line of thrust of the ribs and along the vertical boundary. Table III (Appendix B) provides the distribution of stresses within the bench, in terms of the contact pressure S_r. Figure 14 provides similar data in graphic form.

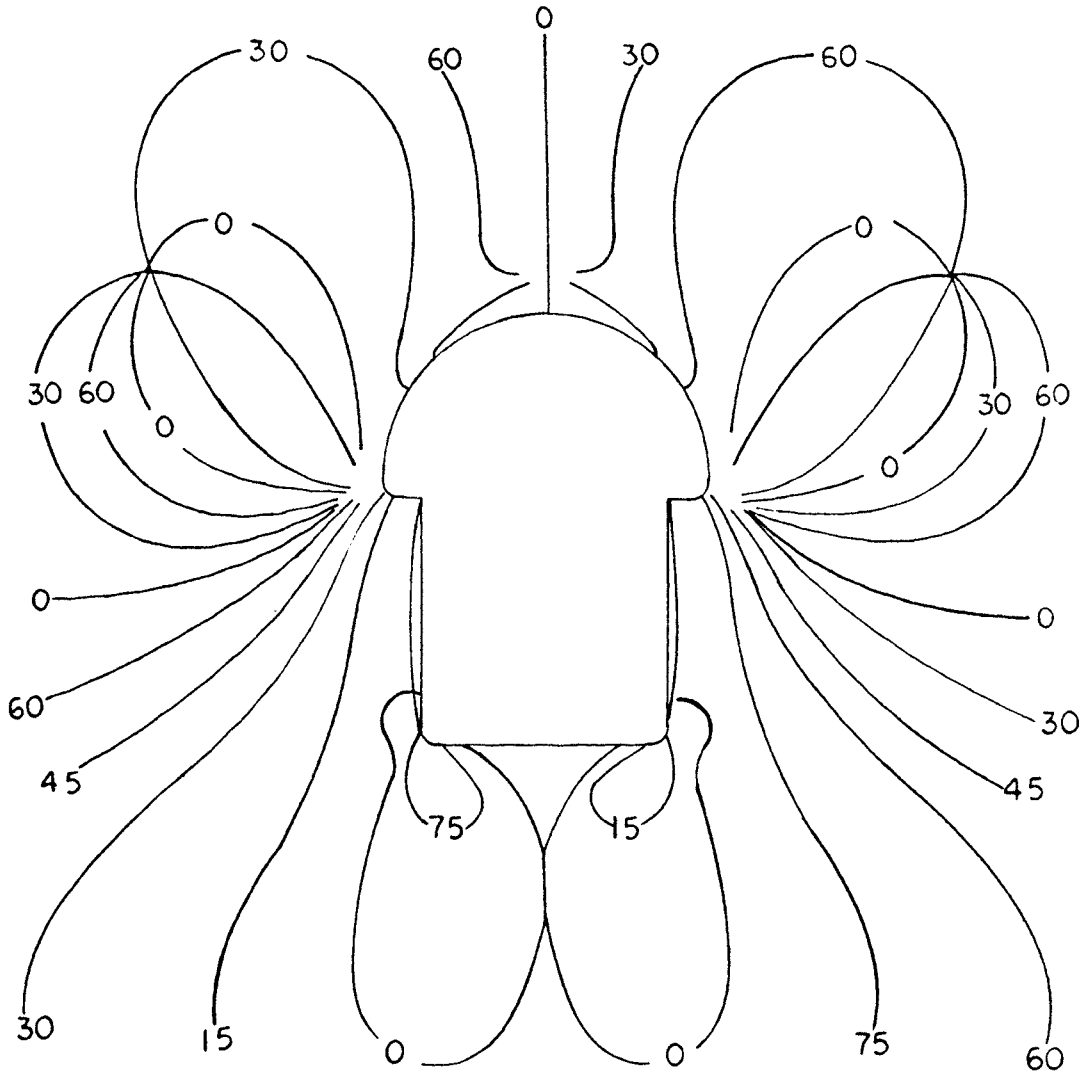

Figure 12. Isoclinics due to rib loading.

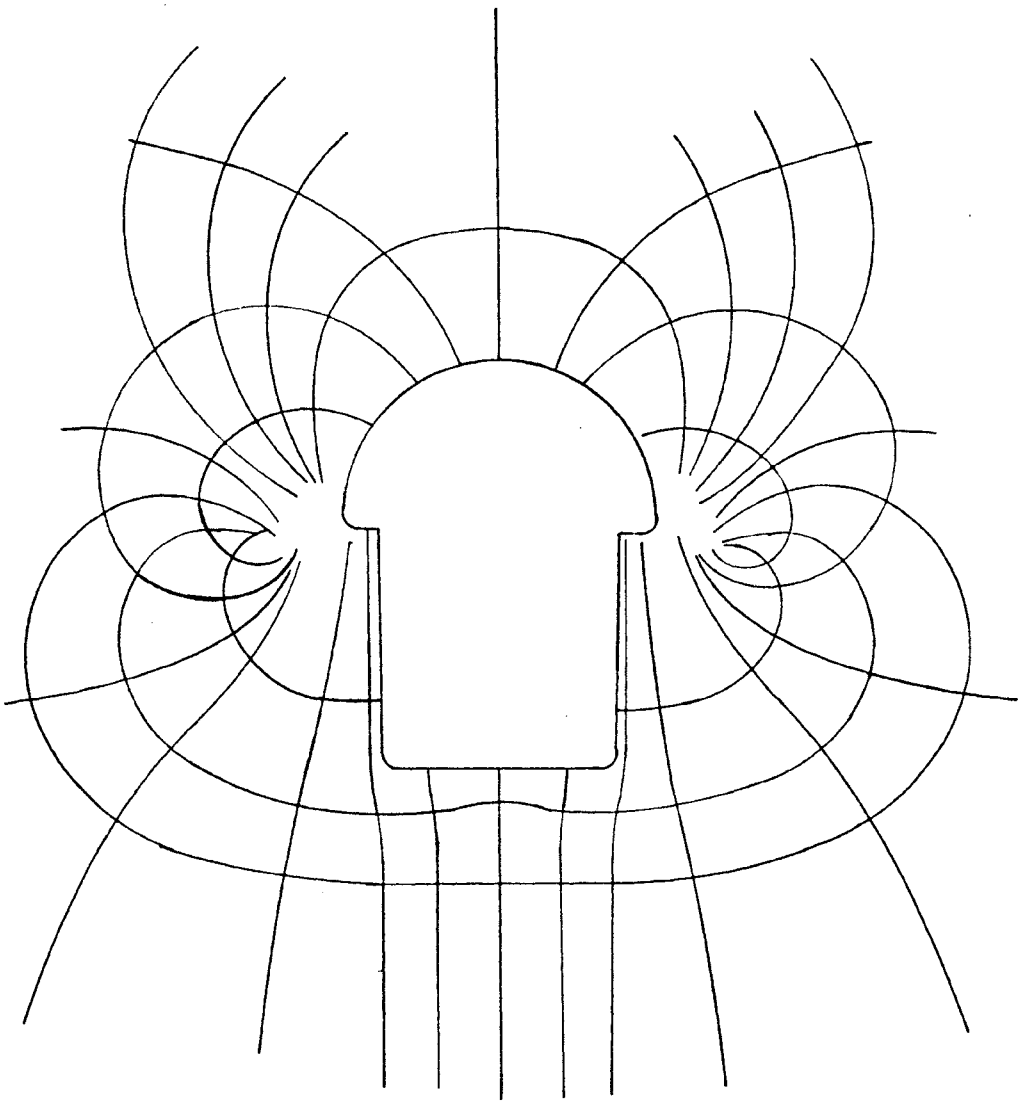

Figure 13. Stress trajectories due to rib loading.

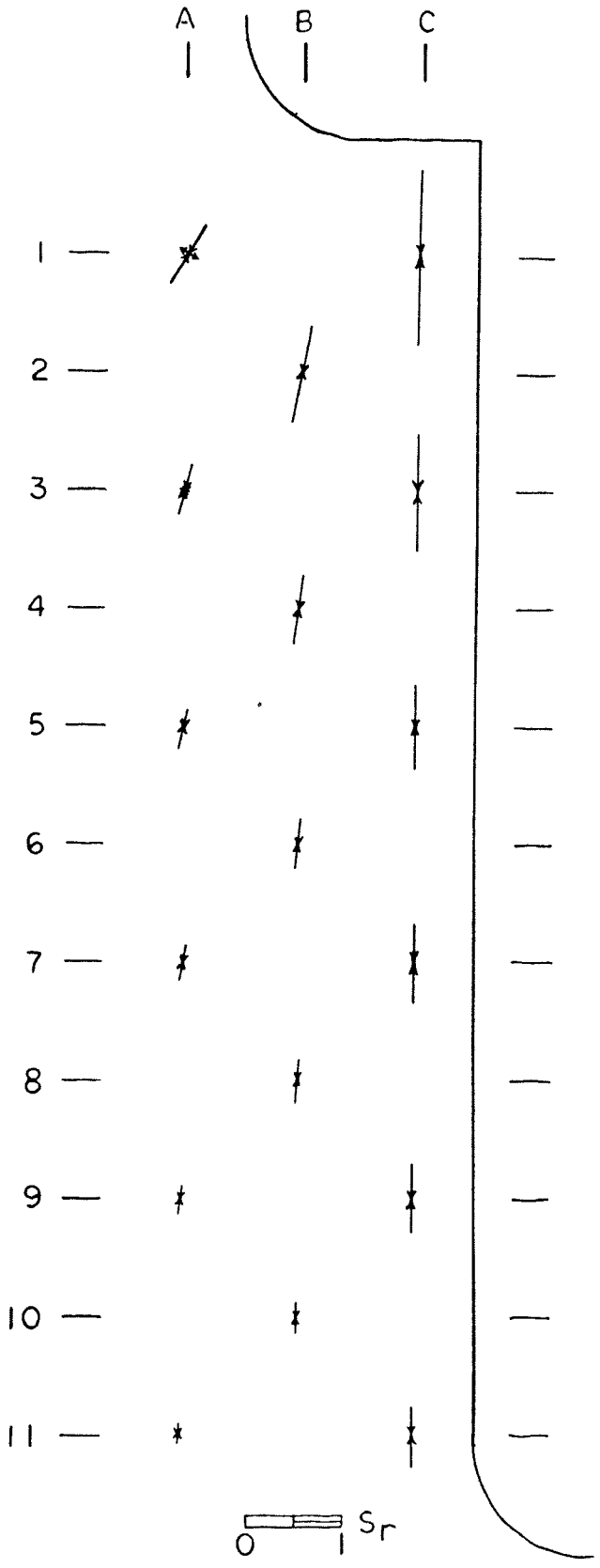

Figure 14. Bench stress due to rib loading.

VI. APPLICATION OF DATA

A. Design of Opening

Assume that an opening is to be constructed in a massive limestone with properties similar to those described in the section on similitude. The opening will be approximately 160 feet high and of the same proportions as the model opening. The limestone has a design strength of 3500 psi (in unconfined compression) and a design tensile strength of 400 psi. The undisturbed vertical stress in the rock at the top of the bench has been determined to be 1000 psi.

Examination of the tangential stress distribution for the opening reveals that the design compressive strength of the limestone would be exceeded. The compressive stresses at the springline would approach 4500 psi ($+4.5\ S_v$) while those at the lower corners would approach 3500 psi ($+3.5\ S_v$). The tensile stresses in the crown and invert would approach -1000 and -1500 psi, respectively, exceeding the design strength of -400 psi. The tensile stress within the rock bench may be expected to reach values in excess of -600 psi ($-0.60\ S_v$) also exceeding the design strength. Obviously, site conditions are not suitable for this opening unless remedial measures are taken.

B. Support System

Assume that the opening is to be excavated in a rock with sufficient strength to withstand the stresses created by the opening, except in the vicinity of the tunnel crown. Steel ribs are to be installed to support the roof of the opening. The experimental data may now be used to evaluate the ability of the rock bench to withstand the induced stresses.

The stresses created by the opening will be added to those induced by the tunnel ribs to determine the final stress within the bench. In practice, it would be necessary to determine the total stress at a number of points within the bench, comparing the final stress at each point with the design strength of the rock.

Assuming that vertical stress field is 1000 psi and that the steel supports will exert a contact pressure of 5000 psi on each bench, the total stress at point A-3 will be determined.

Table II (Appendix A) indicates that at point A-3 the stress created by the opening is:

$$S_1 = +2.46\ S_v = 2480 \text{ psi}$$

$$S_2 = -0.24\ S_v = -240 \text{ psi}$$

$$\theta = 84^\circ$$

Using Mohr's circle or the stress transformation equations, the stresses along the x and y axes can be determined:

$$S_{x_1} = -210 \text{ psi}$$

$$S_{y_1} = -2450 \text{ psi}$$

$$T_{xy_1} = +280 \text{ psi}$$

The stress at point A-3 due to the rib loading is:

$$S_1 = +0.27\ S_r = +1350 \text{ psi}$$

$$S_2 = +0.02\ S_r = +100 \text{ psi}$$

$$\theta = 15^\circ$$

Again using the stress transformation equations, the stress at point A-3 may be written:

$$S_{x_2} = +160 \text{ psi}$$

$$S_{y_2} = +1290 \text{ psi}$$

$$T_{xy_2} = -325 \text{ psi.}$$

Since the stresses due to both loading conditions have now been transformed to their x and y components, they may be added to determine the total stress:

$$S_{x_T} = -50 \text{ psi}$$

$$S_{y_T} = +3740 \text{ psi}$$

$$T_{xy} = -45 \text{ psi.}$$

The principal stresses due to the combined loads are:

$$S_1 = +3742 \text{ psi}$$

$$S_2 = -48 \text{ psi}$$

$$T_{max} = 1895 \text{ psi}$$

These stresses may now be compared with the design strength of the rock to determine the suitability of the design.

VII. CONCLUSIONS

Photoelasticity can accurately predict the behavior of rock only to the extent that the rock behaves as an elastic material. Since the behavior of a rock mass is usually governed more by its discontinuities than by the elasticity of the parent material, photoelastic data must be applied with caution. When applied to underground openings, photoelastic model studies should be used as indications of the relative magnitude and direction of stress rather than as quantitative analyses. Nevertheless, such studies can provide valuable insight into the nature and causes of observed mechanical phenomena.

The tensile stresses which occur in the crown and the floor of the opening are of minor importance. Failure of the rock in the floor of an opening due to horizontal tensile stresses would be difficult to detect and would not affect the stability of the opening or the activity within the opening. The behavior of the roof of an opening is controlled primarily by the orientation, frequency, and persistence of geological discontinuities. In most cases, there are a sufficient number of discontinuities within a rock mass to prevent any accumulation of tensile stresses in the roof of an opening. Most underground openings experience at least minor roof falls; whether these are caused by tension fractures or by geological discontinuities is largely irrelevant.

The critical compressive stress concentration occurs at the springline of the opening and is of the order of 4.5 S_v, the vertical stress. Since an opening of this size and shape is usually excavated in relatively competent rock, this stress concentration will be truly critical only where the vertical stress is relatively high. For rock with a compressive strength

of 3000 psi, the vertical stress must exceed 670 psi, corresponding to a depth of approximately 600 feet. Where this stress concentration is critical, it may be slightly reduced by increasing the height of the arch or by increasing the radius of the fillet. Unfortunately, the shape of the corners is usually controlled more by the condition of the rock than by the operator.

Of primary significance is the occurrence of tensile stresses within the rock bench, reaching a maximum value of $-0.6\ S_v$. The observed phenomena of spalling may now be attributed to tensile failure rather than stress relief, as has previously been hypothesized. Since the tensile strength of rock is usually much lower than the compressive strength, failure of the bench may occur before there is appreciable distress at the springline. It is believed that widening of the bench would merely serve to increase the tensile stresses, and that these can be eliminated only by narrowing or eliminating the rock bench.

In conclusion, the tensile stresses within the rock bench are believed to be the controlling factor in the selection of this opening shape since it is the ability of the bench to withstand the induced stress which makes this design feasible. Using the data in this report, the engineer can evaluate both the stability of the opening and the effect of the support system on the rock bench.

REFERENCES

Abel, John F. Jr., Tunnel mechanics, Quarterly of the Colorado School of Mines, Vol. 62, No. 2, April, 1967.

Frocht, Max M., Photoelasticity, Vol. I and II, John Wiley and Sons, New York, 1941, 1948.

Greenspan, Martin, Effect of a small hole on the stresses in a uniformly loaded plate, Quarterly of Applied Mathematics, Vol. 2, p. 60-71.

Hansen, Peter G., Mimeographed notes for Experimental Stress Analysis II, University of Missouri - Rolla, 1969.

Heller, S. R. Jr., Brock, J. S. and Bart, R., The stresses around a rectangular opening with rounded corners in a uniformly loaded plate, Transactions of the 3rd U.S. Congress on Applied Mechanics, AIME, 1958.

Jessop, H. T. and Harris, F. C., Photoelasticity, principles and methods, Dover Publications, New York, 1950.

Nair, O. B. and Udd, J. E., Stresses around openings in a plate due to biaxial loads through a superpositioning technique, Proceedings of the Rock Mechanics Symposium, University of Toronto, 1965.

Obert, Leonard and Duvall, Wilbur I., Rock mechanics and the design of structures in rock, John Wiley and Sons, New York, 1967.

Obert, Leonard, Duvall, Wilbur I., and Merrill, Robert H., Design of underground openings in competent rock, U.S. Bureau of Mines Bulletin 587, 36 p., 1960.

Panek, Louis A., Stresses about mine openings in a homogeneous rock body, Edwards Brothers Inc. , Ann Arbor Mich. p. 1-50, 1951.

Phillips, H. B., and Zanger, C. N., Stresses around a gallery determined by the photoelastic interferometer, U.S. Bureau of Reclamation Engineering Monograph 12, April, 1952.

Proctor, R. V. and White, T. L., Rock tunneling with steel supports, The Commercial Shearing and Stamping Co., Youngstown Ohio, 1946.

APPENDIX A

PHOTOGRAPHS

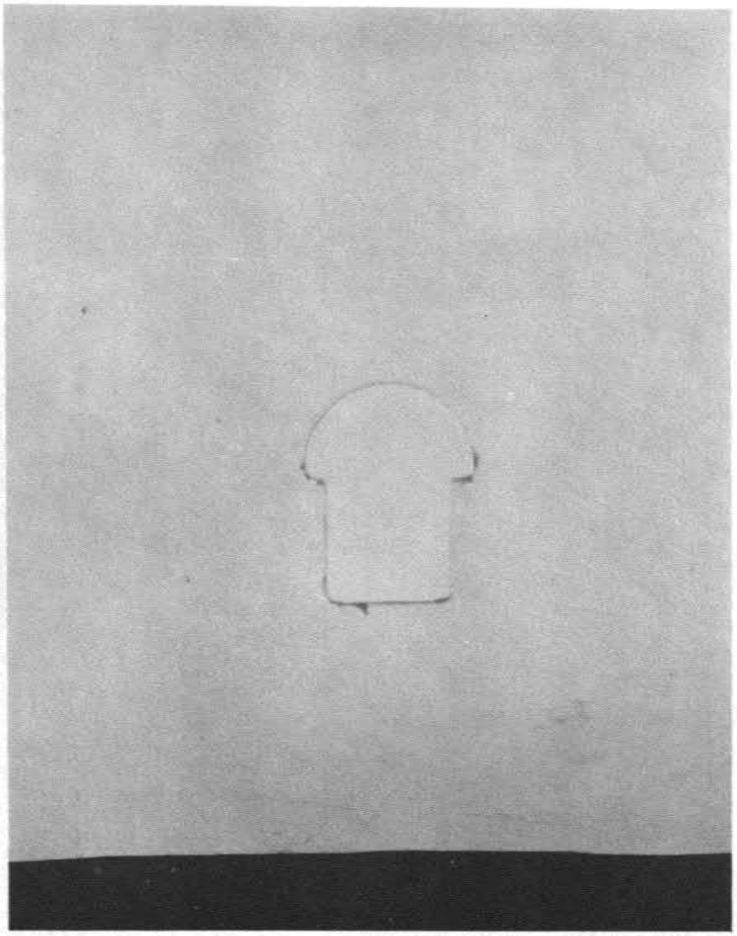

Photograph 1. Completed model viewed through circular polariscope.

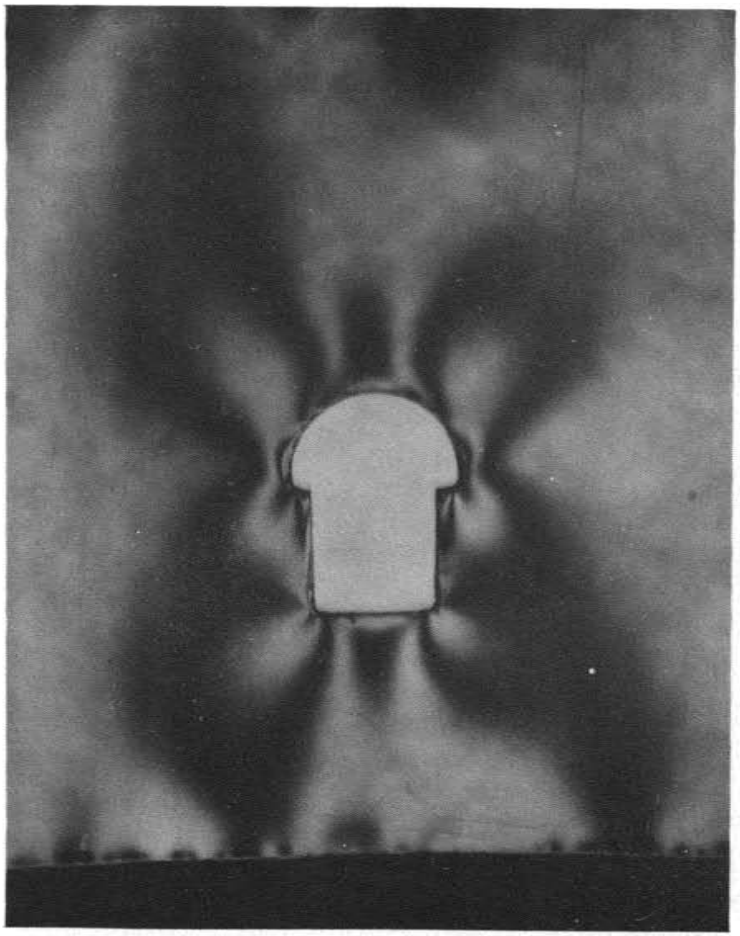

Photograph 2. Half-order isochromatics at 300 rpm.

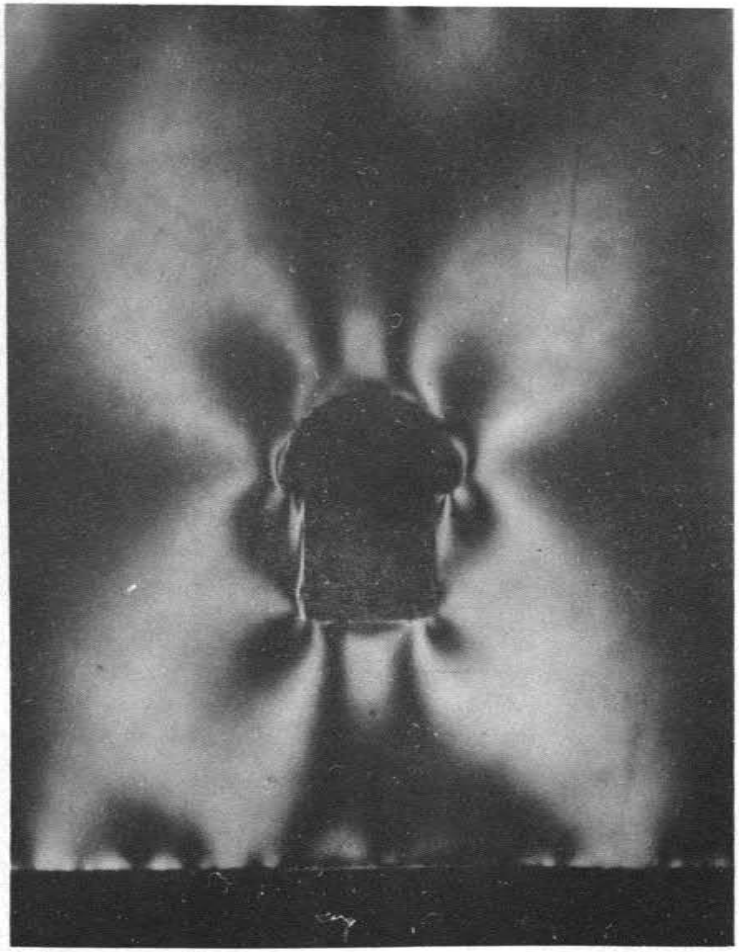

Photograph 3. Integral-order isochromatics at 360 rpm.

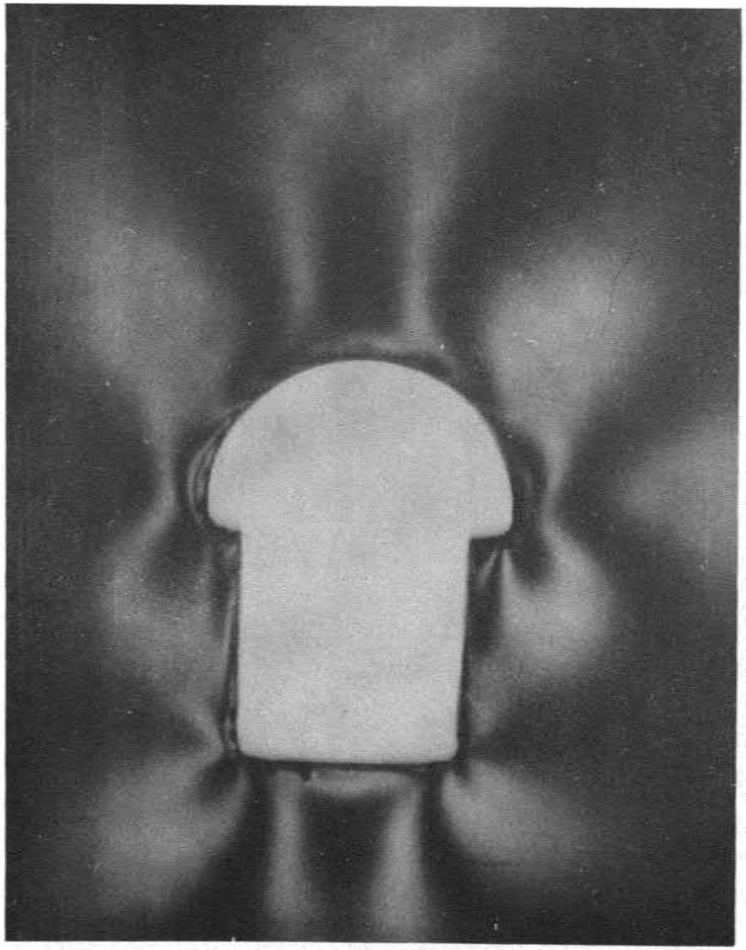

Photograph 4. Enlarged view of half-order isochromatics at 300 rpm.

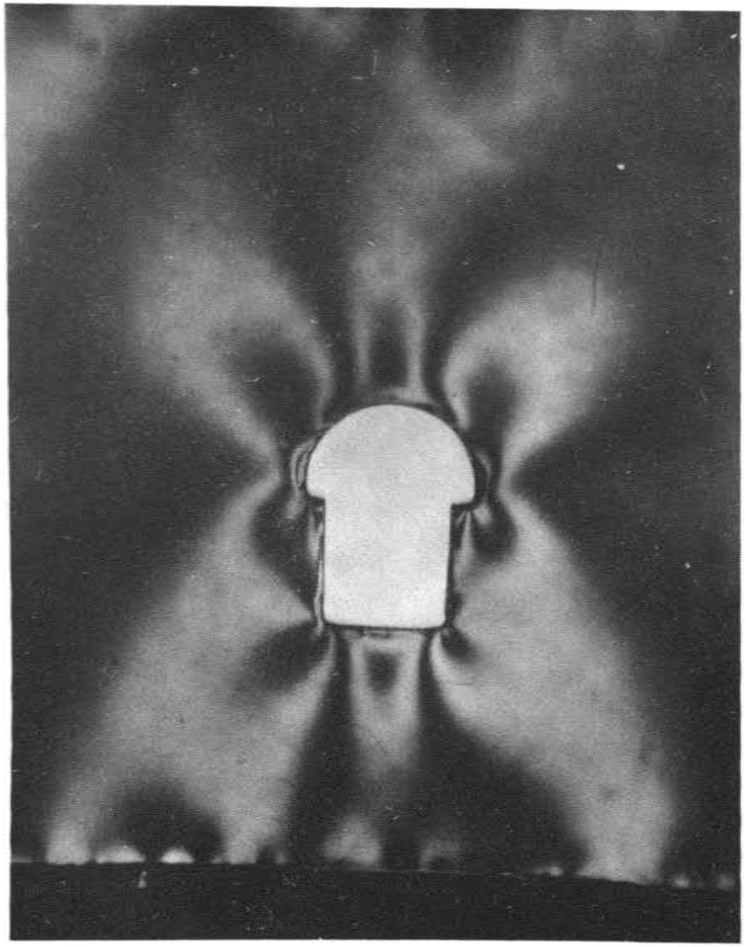

Photograph 5. Half-order isochromatics at 360 rpm.

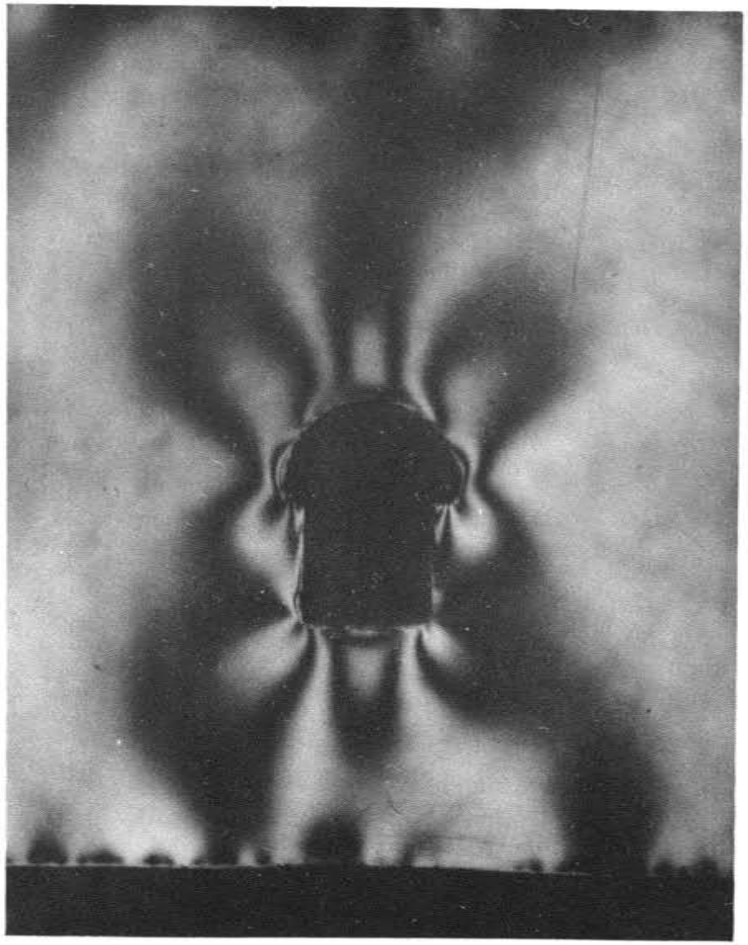

Photograph 6. Integral-order isochromatics at 360 rpm.

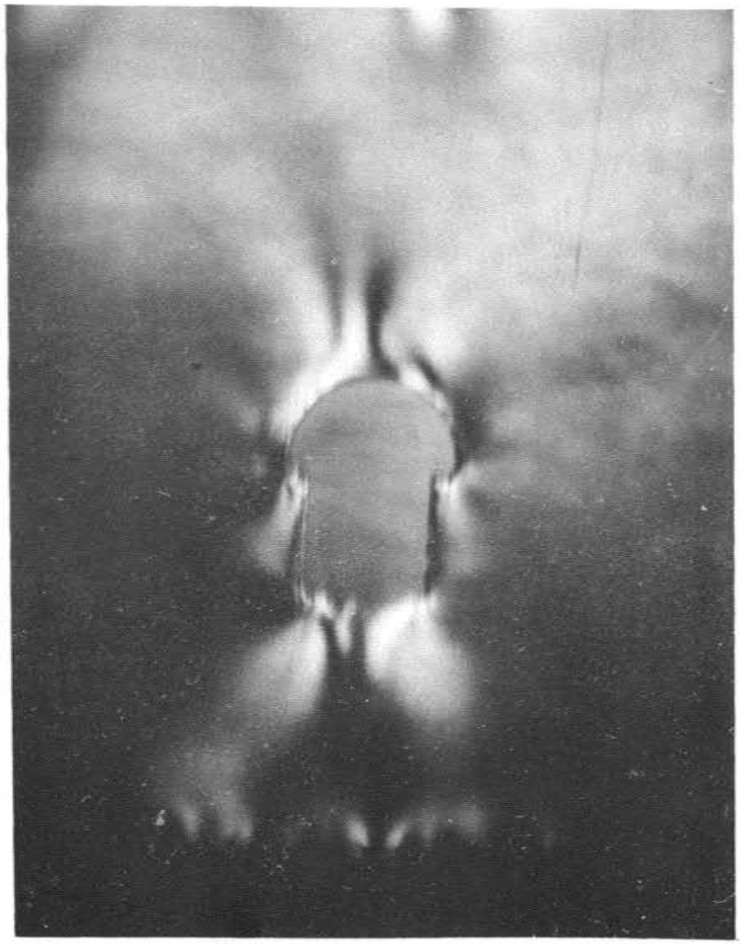

Photograph 7. 0° Isoclinics, using centrifuge.

Photograph 8. 45° Isoclinics, using centrifuge.

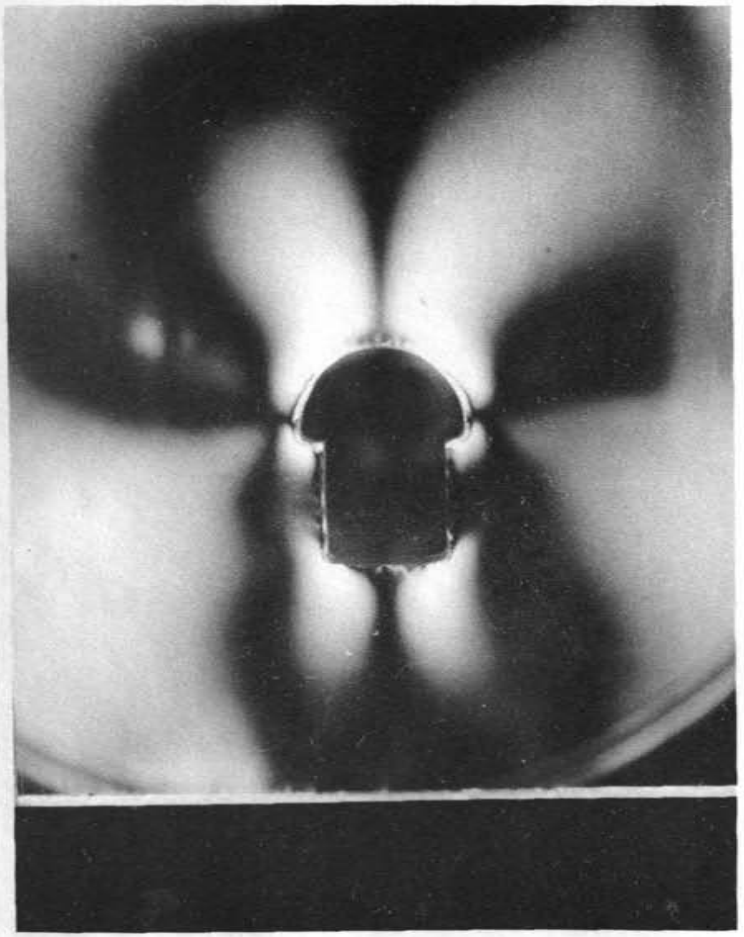

Photograph 9. 0° Isoclinics, using loading frame.

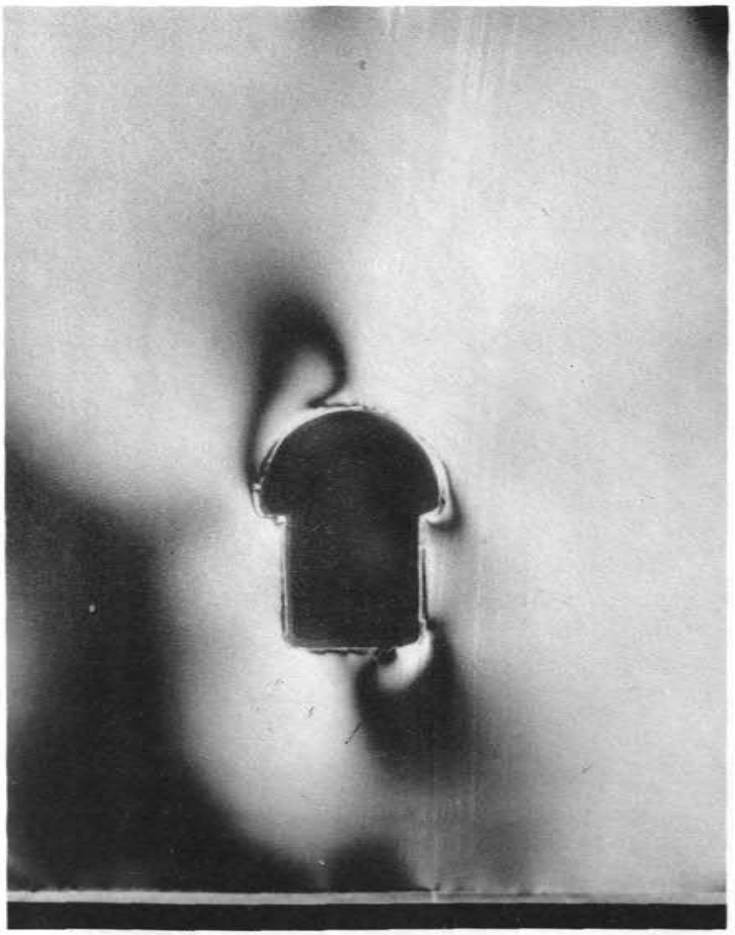

Photograph 10. 15° Isoclinics, using loading frame.

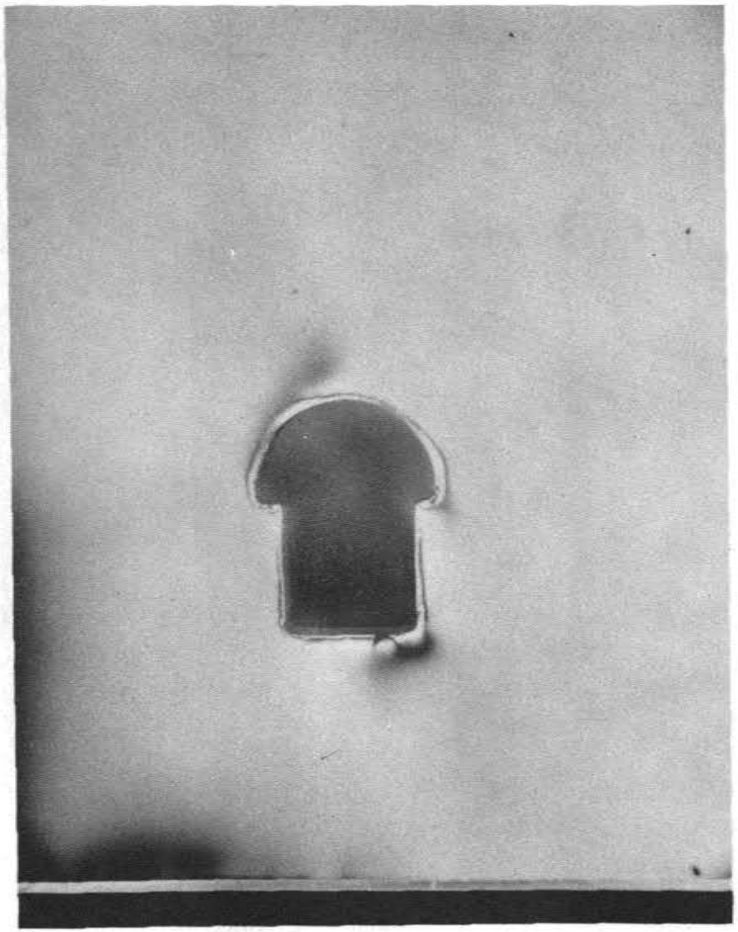

Photograph 11. 30° Isoclinics, using loading frame.

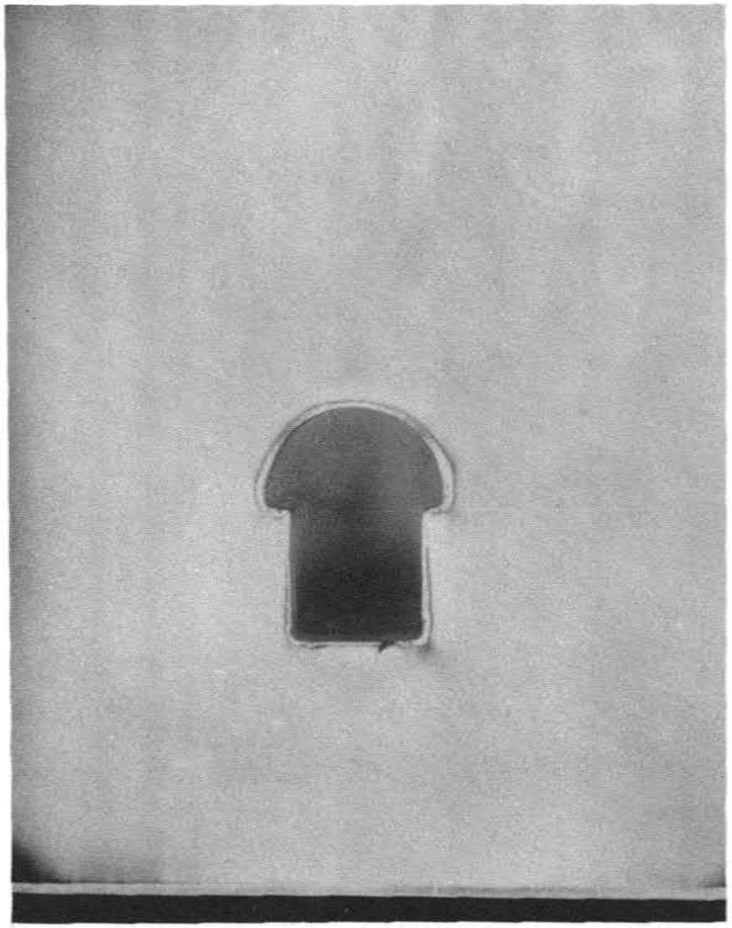

Photograph 12. 45° Isoclinics, using loading frame.

Photograph 13. 60° Isoclinics, using loading frame.

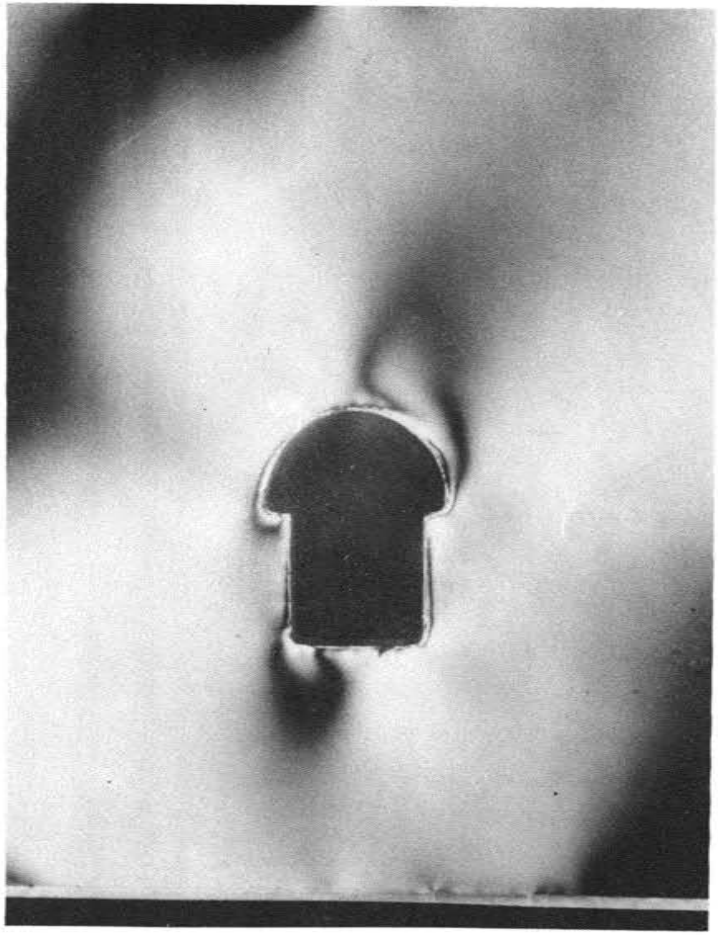

Photograph 14. 75° Isoclinics, using loading frame.

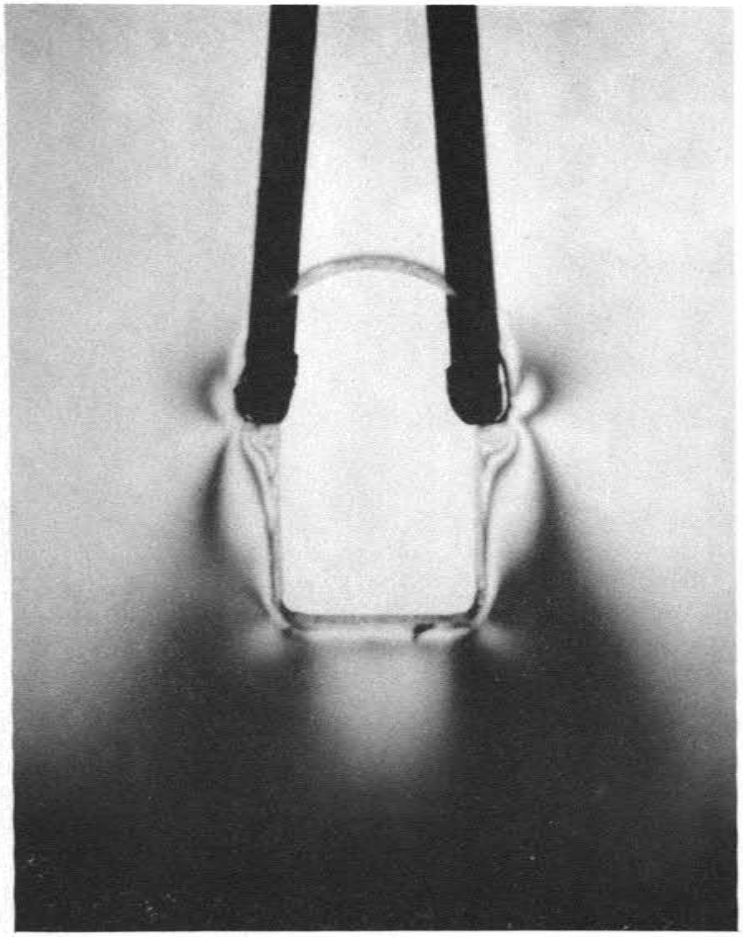

Photograph 15. Half-order isochromatics due to rib loading.

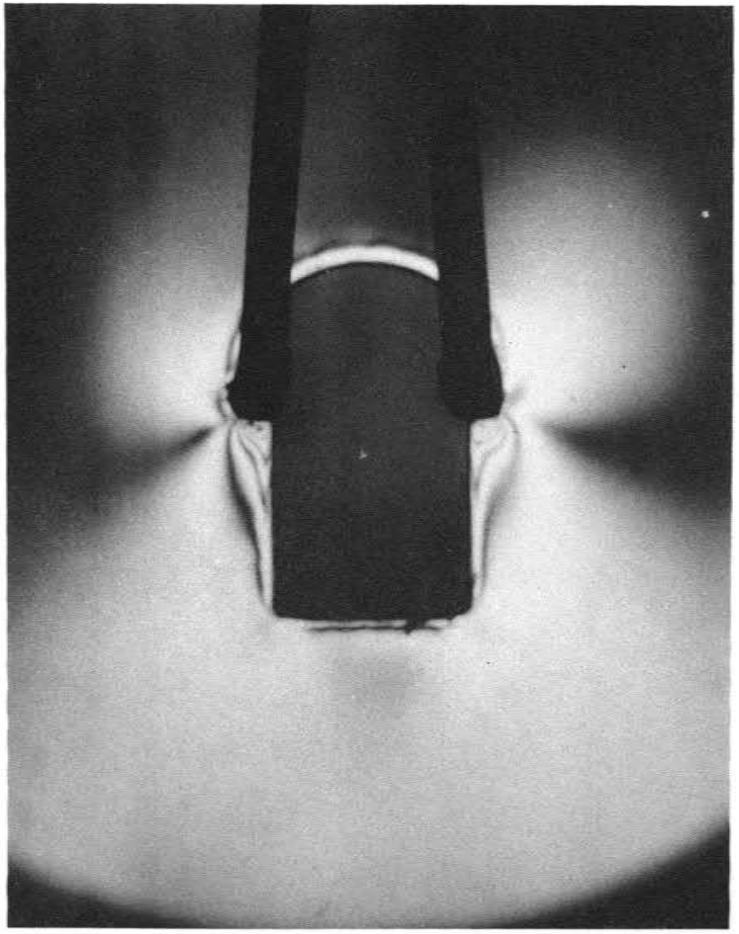

Photograph 16. Integral-order isochromatics due to rib loading.

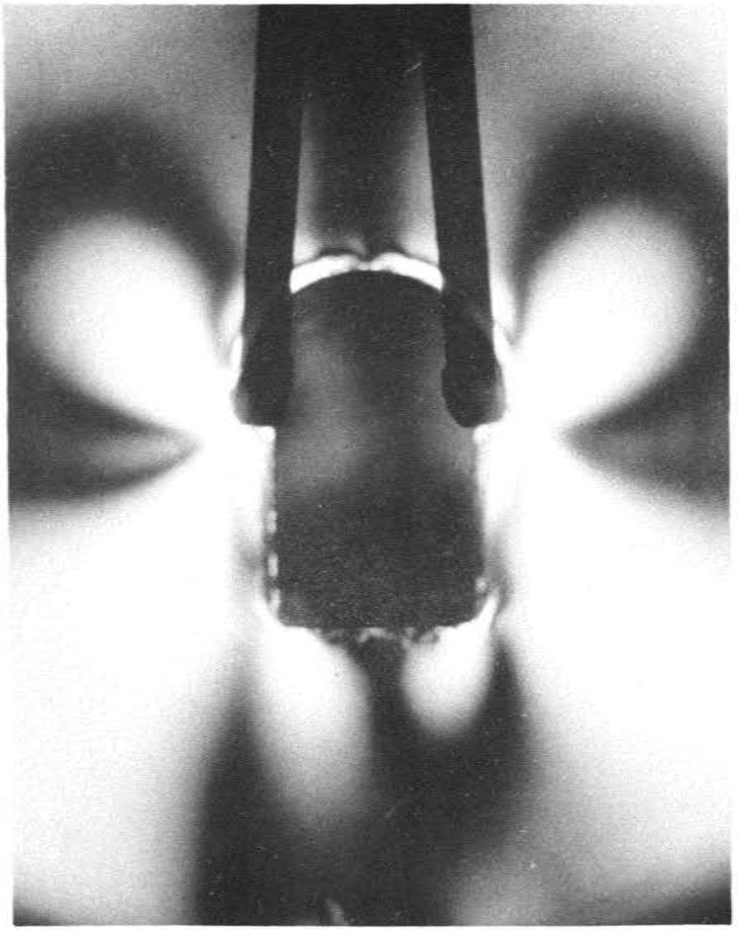

Photograph 17. 0° Isoclinics due to rib loading.

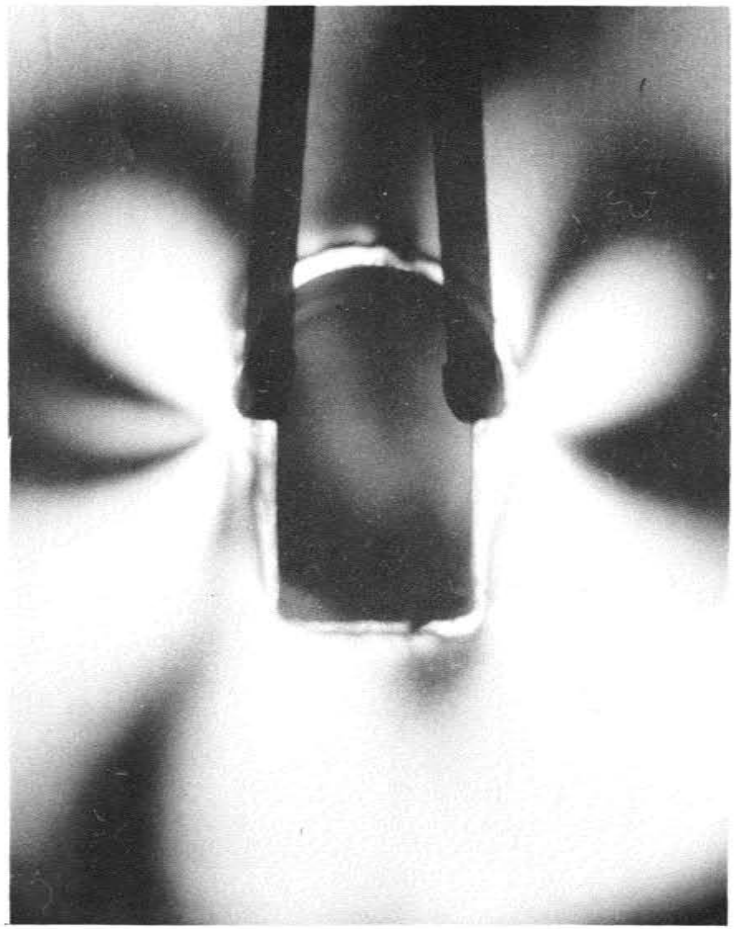

Photograph 18. 15° Isoclinics due to rib loading.

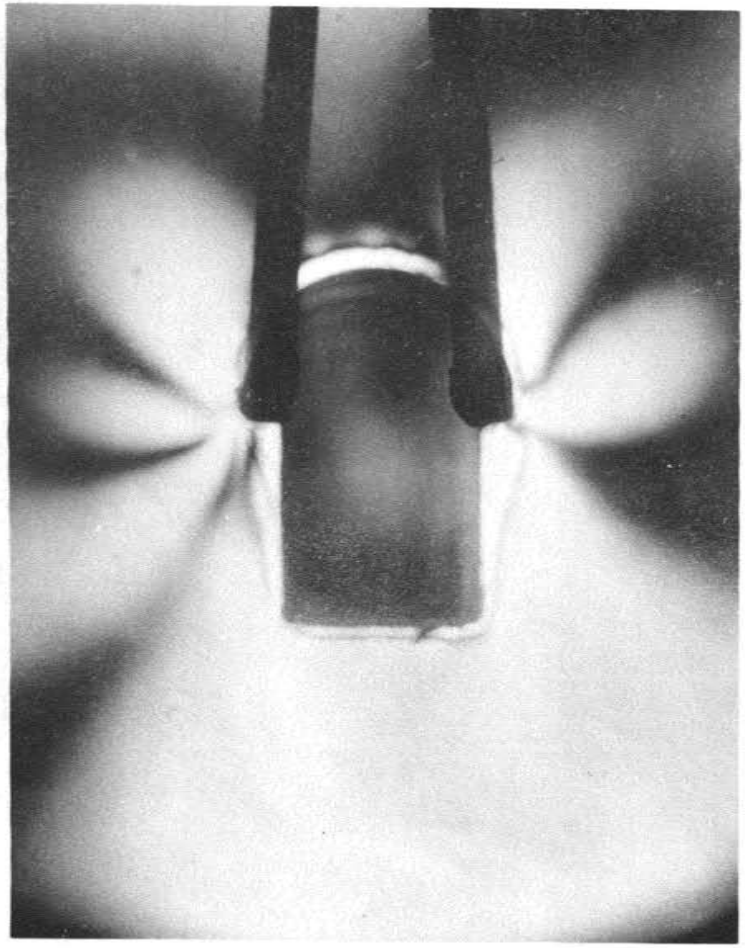

Photograph 19. 30° Isoclinics due to rib loading.

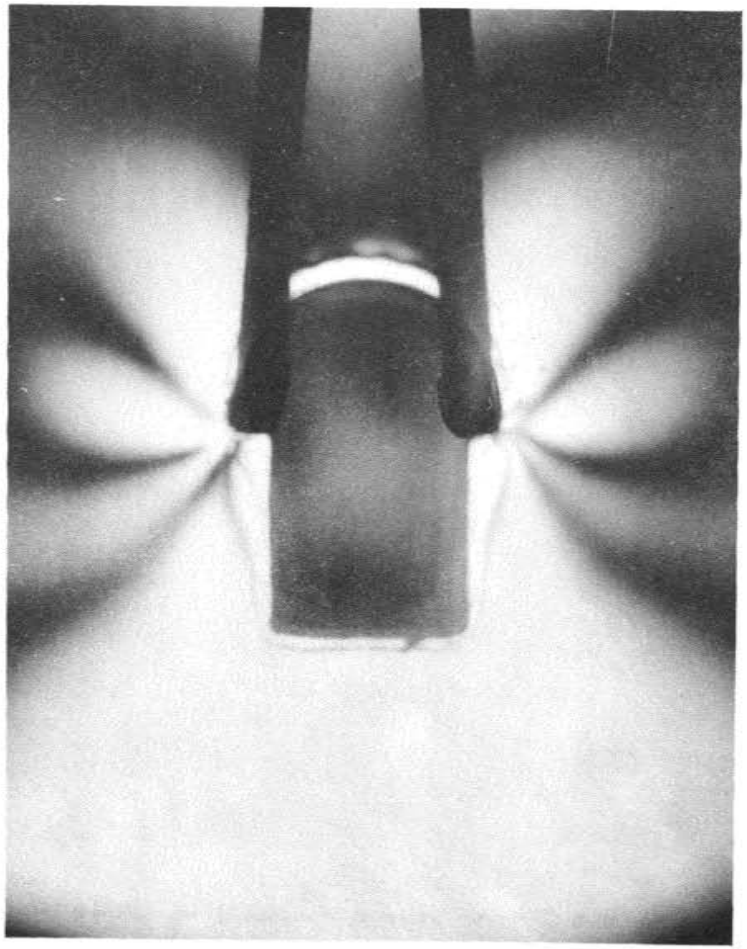

Photograph 20. 45° Isoclinics due to rib loading.

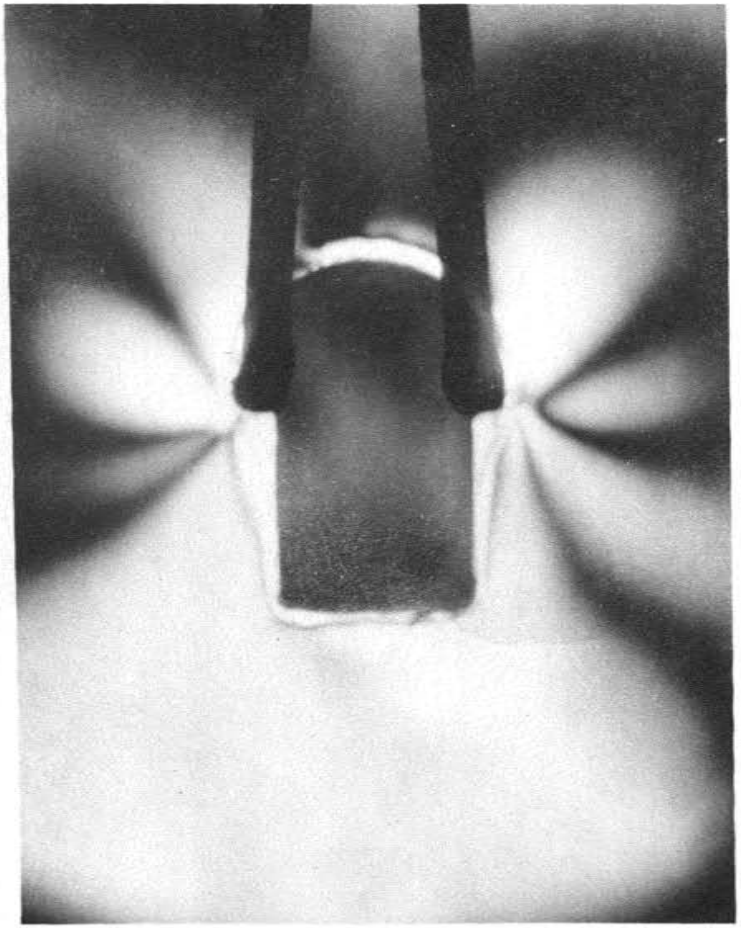

Photograph 21. 60° Isoclinics due to rib loading.

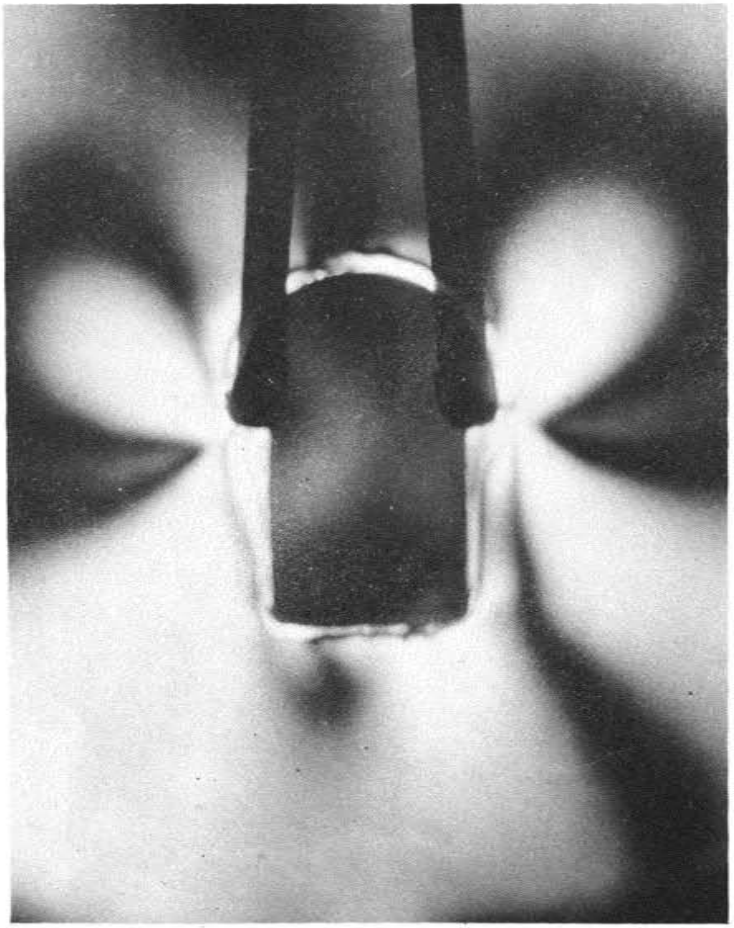

Photograph 22. 75° Isoclinics due to rib loading.

APPENDIX B

TABLES

Table I

Photographic and Polariscope Data

Centrifuge Testing

Photograph	Polariscope	Light	Lens	Exposure
1	Circular-parallel	Monochromatic	0.67x	0.5 sec.
2	Circular-parallel	Monochromatic	0.67x	7 sec.
3	Circular-crossed	Monochromatic	0.67x	7 sec.
4	Circular-parallel	Monochromatic	1.26x	25 sec.
5	Circular-parallel	Monochromatic	0.67x	7 sec.
6	Circular-crossed	Monochromatic	0.67x	7 sec.
7	Linear-crossed	White	0.67x	10 sec.
8	Linear-crossed	White	0.67x	10 sec.

Loading Frame Testing

Photograph	Polariscope	Light	Lens Opening	Exposure
9	Linear-crossed	White	f-8	3 sec.
10	Linear-crossed	White	f-8	3 sec.
11	Linear-crossed	White	f-8	3 sec.
12	Linear-crossed	White	f-8	3 sec.
13	Linear-crossed	White	f-8	3 sec.
14	Linear-crossed	White	f-8	3 sec.
15	Circular-parallel	Monochromatic	f-8	0.5 sec.
16	Circular-crossed	Monochromatic	f-8	0.5 sec.
17	Linear-crossed	White	f-11	4 sec.
18	Linear-crossed	White	f-11	4 sec.
19	Linear-crossed	White	f-11	4 sec.
20	Linear-crossed	White	f-11	4 sec.
21	Linear-crossed	White	f-11	4 sec.
22	Linear-crossed	White	f-11	4 sec.

Table II

Bench Stress Due to Opening

	A	B	C
1.	$S_1 = +2.64\ S_v$ $S_2 = -0.59\ S_v$ $\theta = 70°$	$S_1 = +1.70\ S_v$ $S_2 = -0.32\ S_v$ $\theta = 65°$	$S_1 = +0.92\ S_v$ $S_2 = +0.01\ S_v$ $\theta = 86°$
2.	$S_1 = +2.46\ S_v$ $S_2 = -0.51\ S_v$ $\theta = 77°$	$S_1 = +1.51\ S_v$ $S_2 = -0.31\ S_v$ $\theta = 75°$	$S_1 = +1.49\ S_v$ $S_2 = -0.02\ S_v$ $\theta = 87°$
3.	$S_1 = +2.48\ S_v$ $S_2 = -0.24\ S_v$ $\theta = 84°$	$S_1 = +1.68\ S_v$ $S_2 = -0.145\ S_v$ $\theta = 81°$	$S_1 = +1.95\ S_v$ $S_2 = -0.01\ S_v$ $\theta = 0°$
4.	$S_1 = +2.32\ S_v$ $S_2 = -0.19\ S_v$ $\theta = 0°$	$S_1 = +1.68\ S_v$ $S_2 = -0.14\ S_v$ $\theta = 87°$	$S_1 = +2.12\ S_v$ $S_2 = 0$ $\theta = 0°$
5.	$S_1 = +2.42\ S_v$ $S_2 = 0$ $\theta = 0°$	$S_1 = +1.81\ S_v$ $S_2 = 0$ $\theta = 0°$	$S_1 = +2.26\ S_v$ $S_2 = 0$ $\theta = 0°$
6.	$S_1 = +2.31\ S_v$ $S_2 = 0$ $\theta = 0°$	$S_1 = +2.06\ S_v$ $S_2 = 0$ $\theta = 0°$	$S_1 = +2.46\ S_v$ $S_2 = 0$ $\theta = 0°$
7.	$S_1 = +2.31\ S_v$ $S_2 = 0$ $\theta = 0°$	$S_1 = +2.22\ S_v$ $S_2 = 0$ $\theta = 0°$	$S_1 = +2.62\ S_v$ $S_2 = 0$ $\theta = 0°$
8.	$S_1 = +2.22\ S_v$ $S_2 = 0$ $\theta = 0°$	$S_1 = +2.32\ S_v$ $S_2 = 0$ $\theta = 0°$	$S_1 = +2.82\ S_v$ $S_2 = 0$ $\theta = 0°$
9.	$S_1 = +2.58\ S_v$ $S_2 = +0.46\ S_v$ $\theta = 88°$	$S_1 = +2.64\ S_v$ $S_2 = +0.39\ S_v$ $\theta = 88°$	$S_1 = +3.06\ S_v$ $S_2 = +0.04\ S_v$ $\theta = 88°$
10.	$S_1 = +2.50\ S_v$ $S_2 = +0.50\ S_v$ $\theta = 84°$	$S_1 = +2.74\ S_v$ $S_2 = +0.31\ S_v$ $\theta = 83°$	$S_1 = +3.24\ S_v$ $S_2 = +0.01\ S_v$ $\theta = 87°$
11.	$S_1 = +2.72\ S_v$ $S_2 = +0.41\ S_v$ $\theta = 80°$	$S_1 = +2.66\ S_v$ $S_2 = +0.23\ S_v$ $\theta = 79°$	$S_1 = +2.98\ S_v$ $S_2 = -0.14\ S_v$ $\theta = 75°$

Table III

Bench Stress Due to Rib Loading

	A	B	C
1.	$S_1 = +0.35\ S_r$ $S_2 = -0.08\ S_r$ $\theta^2 = 35°$	$S_1 = +0.74\ S_r$ $S_2 = -0.08\ S_r$ $\theta = 15°$	$S_1 = +0.91\ S_r$ $S_2 = 0$ $\theta = 0°$
2.	$S_1 = +0.38\ S_r$ $S_2 = +0.05\ S_r$ $\theta = 22°$	$S_1 = +0.49\ S_r$ $S_2 = -0.01\ S_r$ $\theta = 11°$	$S_1 = +0.71\ S_r$ $S_2 = 0$ $\theta = 0°$
3.	$S_1 = +0.27\ S_r$ $S_2 = +0.02\ S_r$ $\theta^2 = 15°$	$S_1 = +0.39\ S_r$ $S_2 = 0$ $\theta = 9°$	$S_1 = +0.60\ S_r$ $S_2 = 0$ $\theta = 0°$
4.	$S_1 = +0.21\ S_r$ $S_2 = +0.01\ S_r$ $\theta = 13°$	$S_1 = +0.35\ S_r$ $S_2 = 0$ $\theta = 7.5°$	$S_1 = +0.52\ S_r$ $S_2 = 0$ $\theta = 0°$
5.	$S_1 = +0.20\ S_r$ $S_2 = 0$ $\theta = 12°$	$S_1 = +0.30\ S_r$ $S_2 = 0$ $\theta = 6°$	$S_1 = +0.43\ S_r$ $S_2 = 0$ $\theta = 0°$
6.	$S_1 = +0.19\ S_r$ $S_2 = 0$ $\theta = 11°$	$S_1 = +0.24\ S_r$ $S_2 = 0$ $\theta = 6°$	$S_1 = +0.42\ S_r$ $S_2 = 0$ $\theta = 0°$
7.	$S_1 = +0.18\ S_r$ $S_2 = 0$ $\theta^2 = 10°$	$S_1 = +0.22\ S_r$ $S_2 = 0$ $\theta = 5°$	$S_1 = +0.04\ S_r$ $S_2 = 0$ $\theta = 0°$
8.	$S_1 = +0.16\ S_r$ $S_2 = +0.01\ S_r$ $\theta = 9°$	$S_1 = +0.21\ S_r$ $S_2 = 0$ $\theta^2 = 4°$	$S_1 = +0.38\ S_r$ $S_2 = 0$ $\theta^2 = 0°$
9.	$S_1 = +0.14\ S_r$ $S_2 = +0.01\ S_r$ $\theta = 8°$	$S_1 = +0.20\ S_r$ $S_2 = 0$ $\theta^2 = 2°$	$S_1 = +0.36\ S_r$ $S_2 = 0$ $\theta^2 = 0°$
10.	$S_1 = +0.11\ S_r$ $S_2 = 0$ $\theta = 6°$	$S_1 = +0.18\ S_r$ $S_2 = 0$ $\theta^2 = 2°$	$S_1 = +0.33\ S_r$ $S_2 = 0$ $\theta = 0°$
11.	$S_1 = +0.10\ S_r$ $S_2 = 0$ $\theta^2 = 5°$	$S_1 = +0.16\ S_r$ $S_2 = 0$ $\theta^2 = 0°$	$S_1 = +0.30\ S_r$ $S_2 = 0$ $\theta^2 = 0°$

APPENDIX C

PHOTOELASTICITY

Appendix C

PHOTOELASTICITY

A. Introduction

Photoelasticity measures stress and strain in a model by detecting the change in the index of refraction of light passing through the model. The technique is based on the fact that most transparent isotropic substances become optically anisotropic when subjected to stress. Polarized light, passing through a photoelastic model, will split into two polarized beams which travel in the planes of the principal strains. These beams have different velocities and the resulting retardation is observed and converted into measurements of stress or strain.

B. The Polariscope

The basic tool of photoelasticity is the transmission polariscope. Figures 15 and 16 are schematic diagrams of polariscopes. The basic components of the system are:

a. Light source: both white and monochromatic light are required.

b. Condensing lens: used to collect the light from the source and bring it to a focus at the focal point of field lens c.

c. Field lens: produces a field of parallel light rays.

d. Polarizer: produces plane polarized light. Large field polarizers are made from Polaroid sheet.

e. Quarter-wave plate: converts plane polarized light to circular polarized light.

f. Loading frame: used to apply a load to the photoelastic model. A centrifuge or other devices may be substituted.

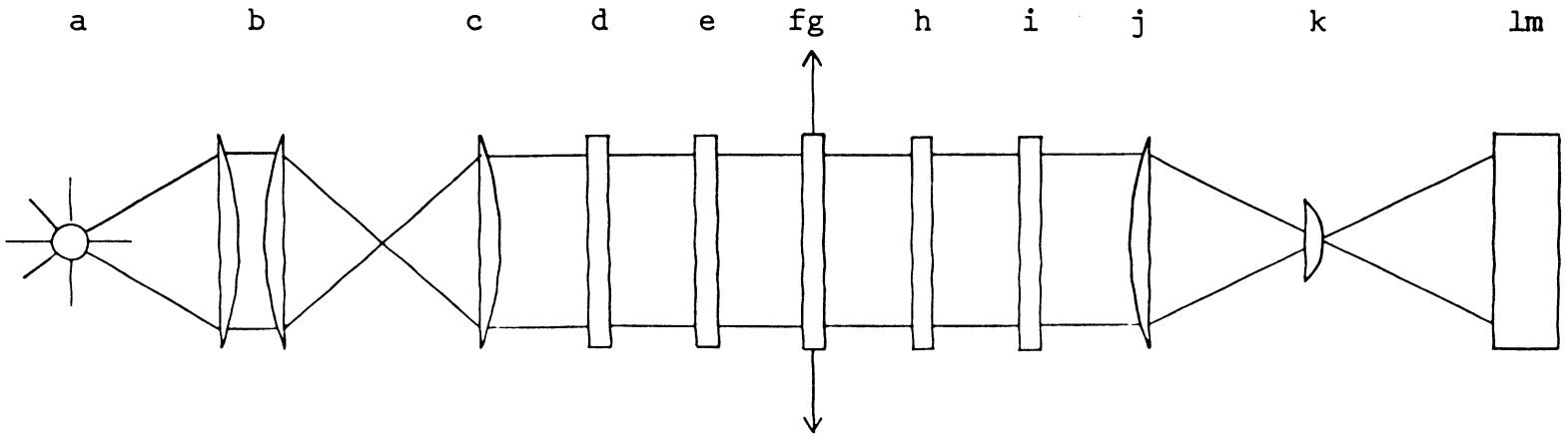

Figure 15. Transmission photoelastic polariscope.

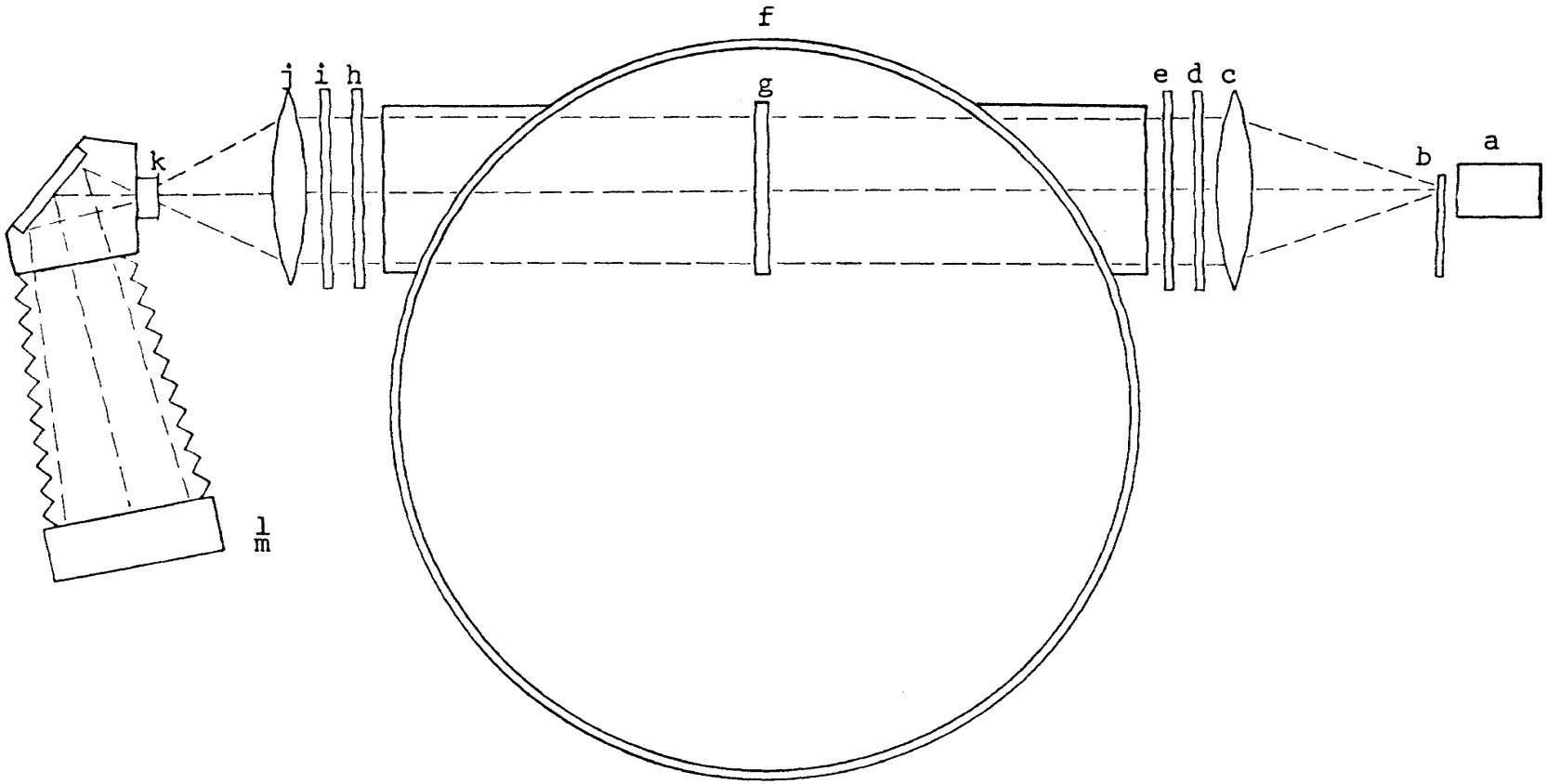

Figure 16. Photoelastic polariscope and centrifuge.

g. Model: may be made of any one of the many photoelastic substances: glass, CR-39, Bakelite, epoxy resins, etc.

h. Quarter-wave plate: the same as e. Both quarter-wave plates should be mounted so they can be independently rotated.

i. Analyzer: identical to the polarizer. The interference effects which occur in the analyzer are observed as isoclinics or isochromatics.

j. Field lens: converges the light beam to the focal point of lens k.

k. Focusing lens: used to focus the image of the model on the viewing screen or camera film.

l. Viewing screen: ground glass or a projecting screen may be used to view the model image.

m. Camera: optional, but extremely useful for precise studies.

C. Interference Phenomena

1. Stress-Optical Laws

A beam of polarized light passing through a stressed sheet of photoelastic material is split into two beams of polarized light. The two beams travel in the planes of the principal stresses at different velocities. The two beams are repolarized by the analyzer to exhibit various interference patterns. These are created by the relative retardation (R) of the two beams of light:

$$R = C(S_1 - S_2)t$$

where C is the stress-optical coefficient and t is the thickness of the material.

For a plane polariscope with crossed analyzer and polarizer, the light emerging from the analyzer has an amplitude:

$$A = a \sin 2\alpha \sin \frac{\pi R}{\lambda}$$

The angle between the planes of the principal stresses and the axes of the polarizer and analyzer is called α and λ is the wave-length of the light. The intensity of the emerging light is proportional to the square of this amplitude and will be zero when

$$a \sin 2\alpha \sin \frac{\pi R}{\lambda} = 0$$

Provided that light is entering the system ($a \neq 0$), extinction, or interference, can occur only if $\sin 2\alpha$ or $\sin \frac{\pi R}{\lambda}$ are equal to zero.

2. Isochromatics

One of the conditions for interference ($\sin \frac{\pi R}{\lambda} = 0$) occurs whenever

$$\frac{\pi R}{\lambda} = n\pi$$

$$\text{or } R = n\lambda$$

where the relative retardation (R) is zero or any integral number (n) of wave-lengths. The effect of this type of retardation will be the appearance of a number of dark lines or bands, called isochromatics. The isochromatic corresponding to n wave-lengths relative retardation is called the isochromatic of the nth order. If the analyzer and polarizer are parallel to one another, extinction occurs when

$$R = \frac{n\lambda}{2}, \frac{3n\lambda}{2}, \frac{5n\lambda}{2}, \text{ etc.}$$

The isochromatics observed through a parallel (light field) polariscope are called half-order isochromatics.

In practice, it is necessary to determine the order (n) of a fringe or isochromatic experimentally. By gradually increasing the load on the model, the first isochromatic to appear on the model can be identified as the first-order isochromatic.

3. Isoclinics

The second condition for interference ($\sin 2\alpha = 0$) occurs whenever $2\alpha = n$, where n is zero or any integer. This occurs when the axes of the analyzer and polarizer (crossed) are parallel to the planes of the principal stresses. The interference band, or isoclinic, marks the location of all points in the plate where the principal stresses are parallel to the analyzer and polarizer. If the analyzer and polarizer are rotated together, still crossed, the patterns of interference will shift, indicating zones where the principal stresses are parallel to the new orientation of the polarizer and analyzer.

Isoclinics intersect only at certain points called isotropic points. At isotropic points, the principal stresses are equal in all directions, i.e. hydrostatic conditions. A singular point is an isotropic point at which the stresses are zero.

Since isoclinics usually do not provide a very clear picture of the orientations of the principal stresses, isostatics, or stress trajectories, are frequently presented. These are prepared from drawings of the various isoclinics and show the direction of one of the principal stresses at any point on the trajectory lines. Two sets of mutually perpendicular stress trajectories can be drawn.

4. The Circular Polariscope

If a stressed plate is viewed through a polariscope without quarter-wave plates, (a linear or plane polariscope) both isochromatics and isoclinics are observed. Since the isoclinics are frequently broad and indistinct, they may obscure the isochromatics. The isoclinics may be eliminated by the use of two quarter-wave plates with their polarizing axes crossed (a circular polariscope).

> "In the circular polariscope, the first quarter-wave plate converts the single plane polarized wave into two equal waves polarized in perpendicular directions, so that even when the axes of the principal stresses are parallel to these directions, there is a wave vibrating parallel to each of the principal stresses and one of these will be retarded on the other." (JESSOP and HARRIS, 1950, p. 69)

D. Fringe Constant

The stress-optic law was previously written as:

$$R = C(S_1 - S_2)t,$$

which can be rewritten as:

$$n\lambda = ct(S_1 - S_2).$$

Therefore:

$$\frac{\lambda}{c} = (S_1 - S_2)\frac{t}{n} = F.$$

The fringe constant (F) is a constant for a particular model and light source and is more commonly used than the stress-optical coefficient C. Since photoelastic materials, even of the same substance, possess varying optical properties, the fringe constant must be determined experimentally for each model.

VITA

Alphonse Camille Van Besien was born on April 18, 1937, in Anamosa, Iowa. He received his primary and secondary education in Kansas City, Missouri. He received the Bachelor of Science Degree from the University of Notre Dame and a Commission in the U.S. Army Reserve, in South Bend, Indiana, in January, 1959.

The author has been employed by the U.S. Army Corps of Engineers since November, 1959 and is a member of the Association of Engineering Geologists. He was selected for the Advanced Study Program of the U.S. Army Corps of Engineers in 1968 and has been enrolled in Graduate School at the University of Missouri - Rolla since September, 1968.

He is married to the former Carol Jean Stoll of Springfield, Missouri. A son, John Christopher, was born on August 11, 1966.